Presented at Summer Institute on Particle Physics, Stanford, California
August 2 - 13, 1976

LBL-5534
c.1

STUDY OF CHARMED MESONS AT SPEAR

Gerson Goldhaber

October 1976

Prepared for the U. S. Energy Research and Development Administration under Contract W-7405-ENG-48

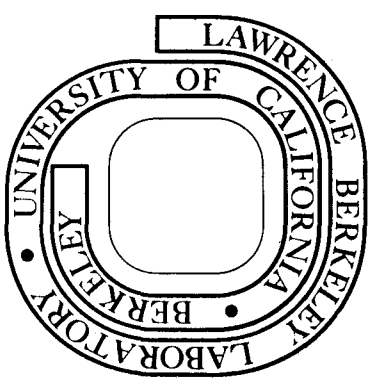

LBL-5534
c.1

DISCLAIMER

LBL-5534

STUDY OF CHARMED MESONS AT SPEAR

Gerson Goldhaber

Department of Physics and Lawrence Berkeley Laboratory
University of California, Berkeley, California 94720

I. PRODUCTION AT SPEAR

The data I will discuss here comes from the SLAC-LBL magnetic detector at SPEAR. This detector as well as event selection techniques have been described earlier,[1] and I will thus confine myself to some details about the time-of-flight system only.

Early in May 1976 we observed a narrow peak in two neutral decay modes[2] $K\pi(1865)$ and $K3\pi(1865)$ based on the study of ~ 29,000 hadronic events from the E_{cm} region 3.9 - 4.6 GeV. In this talk I will discuss this data as well as new data from two additional runs at SPEAR at E_{cm} = 4.028 GeV and E_{cm} = 4.415 GeV, taken during May - June 1976. These consisted of ~ 25,000 and ~ 26,000 hadronic events respectively. The energies were chosen to lie at the two prominent peaks of the R plot ($R = \sigma_{hadron}/\sigma_{\mu\mu}$) shown in Fig. 1.

In June 1976, from a study of the 4.028 GeV data, for which the ratio of signal to background for the new mesons is considerably improved over the earlier 3.9 - 4.6 GeV data, we observed the charged decay mode[3] $K^{\mp}\pi^{\pm}\pi^{\pm}(1876)$.

The entire sample analyzed here thus corresponds to ~ 80,000 hadronic events identified in the detector. In the present analysis we have confined ourselves to hadronic events with three or more observed prongs.

Summary of Data Sample (Preliminary)

E_{cm} (GeV)	Hadronic Events	Integrated Luminosity (nb^{-1})
3.9 - 4.6 pre-May 1976	~ 29,000	~ 1830
4.028	~ 25,000	~ 1280
4.415	~ 26,000	~ 1630
3.9 - 4.6 all	~ 80,000	~ 4740

The Particle Identification Methods by Time of Flight

An important innovation used in this study was the application of time-of-flight (TOF) information to help identify hadrons. The TOF system includes 48 2.4 cm × 20 cm × 260 cm Pilot Y scintillation counters arranged in a cylindrical array immediately outside the tracking spark chambers at a radius of 1.5 m from the beam axis. Both ends of each counter are viewed by Amperex 56 DVP photomultiplier tubes (PM); anode signals from each PM are sent to separate TDC's, ADC's, and latches. Pulse height information is used to correct times given by the TDC's. The collision time is derived from a pickup electrode that senses the passage of the 0.2 ns long beam pulses; the period between successive collisions is 780 ns. Run-to-run calibrations of the TOF system are performed with Bhabha scattering ($e^+e^- \rightarrow e^+e^-$) events. The rms resolution of the TOF system is $\sigma_t = 0.4$ ns.

Typical time difference between a π and a K in the Kπ signal is only about 0.5 ns. We have used the following two techniques to extract the best possible information on particle identity. To apply these methods, tracks are required to have good timing information from both PM's, consistent with the extrapolated position of the track in the counter.

A. Direct Particle Identification by TOF

In this method we calculate two χ^2 values for each observed track. The first is related to the probability that the track is a π, (χ^2_π) and the second to the probability of the track being a K, (χ^2_K). Here χ^2_i is defined by:

$$\chi^2_i = (t_i - t_M)^2/\sigma_t^2$$

where $i = \pi, K$; t_i is the time calculated for mass i from measured momentum; t_M is measured TOF. If the track satisfies the criteria $\chi^2_K < 3$, $\chi^2_K < \chi^2_\pi$ the track is called a K. If $\chi^2_\pi < \chi^2_K$ the track is called a π; the track is also called a π when no reliable TOF information is available as when, for example, more than one track hits the TOF counter. There are also a small number of nucleons and antinucleons which have been identified

but these do not play a part in the present analysis.

B. The Weight Method

In the weight method each track is assigned a weight corresponding to its probability of being a π and a second weight corresponding to its probability of being a K. These are determined from the measured momentum and TOF assuming a Gaussian probability distribution with standard deviation 0.4 ns. Tracks with net (π plus K) probability less than 1% are rejected. (This eliminates most of the nucleons.) Then, the relative π-K probabilities are renormalized so that their sum is unity, and two-particle combinations are weighted by the joint probability that the particles satisfy the particular π or K hypothesis assigned to them. In this way, the total weight assigned to all $\pi\pi$, Kπ, and KK combinations equals the number of two-body combinations and no double-counting occurs.

To be more specific, we define

$$W_\pi \propto e^{-\chi_\pi^2/2}$$

and $$W_K \propto e^{-\chi_K^2/2}$$

with the normalizing condition

$$W_\pi + W_K = 1 \quad .$$

In the study of the two-body system, for example, each pair of particles with total charge zero gets entered into three graphs:

in $M(\pi^\pm\pi^\mp)$	we enter	$W_{\pi_1} W_{\pi_2}$
in $M(K^\pm\pi^\mp)$	we enter	$W_{K_1} W_{\pi_2}$ and $W_{\pi_1} W_{K_2}$
in $M(K^\pm K^\mp)$	we enter	$W_{K_1} W_{K_2}$.

In our earlier publications[2,3] we have used method B, the weight method. This method allowed us to give a quantitative assessment of the reliability of the K particle assignments in Kπ(1865). In what follows we will use method A which lends itself more readily to the study of scatter plots. We will also show a comparison between the two methods which demonstrates that for the study of mass plots they do not differ in any essential features.

C. Summary and Nomenclature

At the moment we have no "rigorous proof" that we are indeed dealing with charmed mesons.[4] However, every clue we have uncovered, so far, points in the direction of charm. It is becoming clear that we are dealing with those particles which are correlated with the broad $\psi(4.1)$ resonance and thus very likely with the property that is still "hidden" at the lower energies corresponding to the ψ/J and ψ'.

I will discuss the following about the new particles we have observed:

a. Observation of a threshold: $E_{th} > 3.1$ GeV.

b. Associated production: the particles are produced exclusively in association with another particle of equal or larger mass.

c. Exotic final state: the charged particle decays into an exotic final state. Incidentally, this is the first clearly established case of an exotic final state.

d. Experimental width: from the direct mass measurement of $K\pi(1865)$ we showed that the width is $\Gamma < 40$ MeV/c^2; by including information on the recoil system this can now be reduced to $\Gamma < 5$ MeV.

e. I-spin multiplet: the proximity in mass of the neutral and charged particles in <u>both</u> the ground state <u>and</u> first excited state is evidence that we are dealing with I-spin multiplets.

f. Parity violation in the decay: from a comparison of $K\pi\pi$ and $K\pi$ we give evidence for parity violation, and hence weak decay.

g. Search for Cabibbo forbidden decay modes: we note an indication, in the $\pi^+\pi^-$ channel, at the 1.5 standard deviation level (i.e., not statistically significant).

h. Semi-leptonic decay modes: evidence for these from work at DESY was presented at this Topical Conference.[5]

I could now proceed and call these new particles M^o, M^+, M^{o*}, M^{+*}, etc. where M stands for a new meson, but I will not do so. For clarity and ease of comparison I will use the nomenclature D^o, D^+, etc. introduced

for charmed particles,[4] with the understanding that we do not have complete proof as yet[6] that our observed particles are indeed the mesons of charm theory. Our situation is somewhat analogous to the case of the discovery of the Ω^-. The observed particle has most of the properties predicted for the 10th baryon of the Δ-decuplet while to date no spin and parity measurements are available to check the theoretical prediction $J^P = 3/2^+$.

II. THE ESTABLISHED DECAY MODES

A. Threshold Behavior for the $K^{\mp}\pi^{\pm}$ Decay Mode

In Fig. 2 we show the $K^{\mp}\pi^{\pm}$ mass distribution for three energy regions: the ψ/J, the ψ', and the $E_{cm} = 3.9 - 4.6$ GeV region. The $K^*(890)$ signal shows up clearly in all of them; however the $K\pi(1865)$ signal occurs only for the 3.9 - 4.6 GeV region. Figure 3 shows the $M = 1500 - 2500$ MeV/c^2 region in detail. In these figures the ψ data corresponds to $\sim$ 150,000 hadronic events and the ψ' data to 350,000 hadronic events. We note that of these $\sim$ 72,000 hadronic events correspond to second-order electromagnetic interaction and these at least could be a source for the $K\pi(1865)$ signal. We consider the absence of any such signal a clear indication that the $K\pi(1865)$ does not get produced below a threshold energy E_{th}. Thus $E_{th} > 3.1$ GeV. In Figs. 2, 3 we also show the $E_{cm} = 4.028$ GeV data. For this energy the signal-to-background ratio is much larger than for the overall 3.9 - 4.6 GeV region. The $K\pi(1865)$ particle thus appears specifically associated with the peak in R.

In Fig. 4 we show the $K\pi$ signal for all the $E_{cm} = 3.9 - 4.6$ GeV data with a cut on the recoil mass at $M_{recoil} > 1800$ MeV. This selection tends to reduce the background while the signal remains unaffected. Also shown in Fig. 4 are the kinematic reflections in the "$\pi^+\pi^-$" and "K^+K^-" mass distributions which occur because of K misidentification or lack of TOF information, in which case the track is assigned the pion mass. With the present statistics we note clear "kinematic reflection"

signals at 1740 MeV/c^2 for "$\pi\pi$" and 1990 MeV/c^2 for "$K\bar{K}$." We note that the momentum of the two-body system in such a kinematic reflection signal is not altered by the mass assignment to the track. We will make use of these additional events below in connection with the recoil spectrum.

The $K^{\mp}\pi^{\pm}$ signal is taken from the experimental mass distribution region $M(K\pi) = 1820 - 1900$ MeV/c^2. Background is estimated from two equal width side bands $M(K\pi) = 1700 - 1780$ MeV/c^2 and $M(K\pi) = 1940 - 2020$ MeV/c^2, a total of twice the width of the signal region. This gives a total signal after appropriate background subtraction ($\frac{1}{2} N_{bgnd}$) of 340 ± 47 events. The "$\pi^+\pi^-$" and "K^+K^-" reflection signals are obtained in a similar fashion and give signals of 159 ± 30 and 46 ± 11 events respectively. Thus if we ascribe all these three contributions to $K\pi(1865)$ we get 545 ± 57 events.

B. The $(K3\pi)^0$ Decay Mode

In Fig. 5 we show the $K^{\mp}\pi^{\pm}\pi^+\pi^-$ mass distribution. The $K3\pi(1865)$ signal suffers from a much more severe background problem than the $K\pi(1865)$ signal. We will comment on this in connection with the recoil mass study below. The $K3\pi$ signal was determined for the mass interval 1860 - 1900 MeV/c^2 with two equal side bands for background determination. We find 325 ± 67 events in the signal after background subtraction.

C. The Charged Exotic Decay Mode $K^{\mp}\pi^{\pm}\pi^{\pm}(1876)$

In Fig. 6 we show a comparison of the exotic decay mode $K^{\mp}\pi^{\pm}\pi^{\pm}$ and the non-exotic mode $K^{\mp}\pi^+\pi^-$.

Here "exotic" stands for the fact that the I-spin of the final state is $I = 3/2$ or $5/2$ rather than $I = 1/2$ as is the case for all known K^*'s. Such a final state cannot be formed out of a $q_i\bar{q}_j$ pair where here q_i ($\bar{q}_j$) stands for any of the three "old-fashioned" quarks (anti-quarks). Another way of describing the "exotic" nature of this final state is that the charge of the K is opposite to the charge of the entire $K\pi\pi$ final state. In terms of the charm model[4] the Cabibbo-favored decays involve

a c-quark transforming into an s-quark with $\Delta C = \Delta S$. Thus the D^+ with $C = 1$ and $S = 0$ decays to a system with $C = 0$, $S = -1$ and positive charge, which is exotic. The exotic $K\pi\pi$ signal was determined from the mass interval 1840 - 1920 MeV/c^2. Here background estimates come from the non-exotic channel over the same mass interval, scaled by 1/2. We find 160 ± 35 events in the signal after background subtraction.

III. THE RECOIL SYSTEMS

We find that the $(K\pi)^o$, $(K3\pi)^o$ and $K^{\mp}\pi^{\pm}\pi^{\pm}$ signals are associated with a very distinct recoil spectrum. This can be illustrated in a scatter plot of the final state mass M versus the recoil mass M_{recoil}. In Fig. 7 we show the scatter plot for the $K^{\mp}\pi^{\pm}$ mass distribution and in Fig. 8 for the $K^{\mp}\pi^{\pm}\pi^{\pm}$ mass distribution. The scatter plots shown correspond to the E_{cm} = "4.1" GeV region; i.e., $E_{cm} = 3.9 - 4.25$ GeV, including the data at 4.028 GeV. We note a strong correlation between M and M_{recoil}. This is in agreement with the charm theory expectation that M is essentially a δ-function, on our energy scale, and thus the observed width in M is entirely due to our instrumental resolution. Thus when the measured M value is too large the corresponding M_{recoil} value is too small and vice versa. This then gives rise to the observed correlation. Here M_{recoil} is defined by:

$$M^2_{recoil} = (E_{cm} - \sqrt{p^2 + M^2})^2 - p^2$$

where M and p are the measured effective mass and momentum of the final state considered. Alternately if we consider M as a δ-function, we can substitute a nominal fixed value of $M_{K\pi} = 1865$ MeV and $M_{K\pi\pi} = 1872$ MeV for M respectively.

In Fig. 9a we show the M_{recoil} distribution as measured directly and in Fig. 9b with $M_{K\pi}$ fixed for all the data. In Fig. 9a only the $K\pi$ signal with identified K mesons is shown. On the other hand in Fig. 9b we have also added in the signal from the "$\pi^+\pi^-$" and "K^+K^-" kinematical reflections illustrated in Fig. 4. This is possible as only the experimental quantities

E_{cm} and the momentum p are used to calculate M_{recoil}. The addition of these signals increases the available statistics, but more important, removes biases due to the fact that the reliability of K identification decreases with increasing K momentum. In the distributions in Figs. 9a and 9b the corresponding background has been subtracted. The background was evaluated from the population of two bands on either side of the signal. In Fig. 9a the background bands were subtracted directly without concern for slightly different kinematical boundaries. In Fig. 9b M_{recoil} for the background events was evaluated with the same fixed $M_{K\pi}$ value. This "scales" the kinematic boundaries. Because of the subtraction procedure the statistical errors corresponding to the histograms in Fig. 9 are not given by $\sqrt{N}$ but rather by $\sim\sqrt{1.2N}$ to $\sim\sqrt{1.8N}$.

Some caution must be used in interpreting the four prominent structures in Fig. 9b. Namely, we must remember that the data samples added together in this figure have a highly non-uniform integrated luminosity distribution from E_{cm} = 3.9 - 4.6 GeV. In particular the second and third peaks come largely from the 4.028 GeV data. We observe peaks in M_{recoil} at $\sim$ 1860 MeV/c^2, $\sim$ 2005 MeV/c^2, $\sim$ 2145 MeV/c^2 and $\sim$ 2430 MeV/c^2. Of these the fourth peak is still being studied. An interpretation suggested[7] for the first three peaks is as follows:

$$e^+e^- \rightarrow D^0\overline{D^0} \qquad (1)$$

$$e^+e^- \rightarrow D^0\overline{D^{*0}} \text{ and charge conjugate} \qquad (2)$$

$$e^+e^- \rightarrow D^{*0}\overline{D^{*0}} \ . \qquad (3)$$

A priori, an alternate possibility exists for the third peak; viz.,

$$e^+e^- \rightarrow D^0\overline{D^{**0}} \text{ and charge conjugate} \ . \qquad (3')$$

We will discuss these interpretations in more detail below and in particular show evidence for the strong preference of interpretation (3) over (3'). The recoil spectrum against the $(K3\pi)^0$ mass peak shows consistent features (not shown here) but suffers statistically from the very substantial background subtraction.

In Fig. 10 we show the corresponding M_{recoil} distribution for the exotic channel $K^{\mp}\pi^{\pm}\pi^{\pm}$. In this case the background is deduced from the non-exotic channel $K^{\pm}\pi^{+}\pi^{-}$. In this case we again have a more severe background subtraction as well as a lower statistical significance on the signal (~ 160 events). The very prominent peak observed at M_{recoil} ~ 2012 MeV/c^2 can be interpreted as

$$e^+e^- \rightarrow D^+D^{*-} \text{ and charge conjugate .} \qquad (4)$$

There are indications in the data for the presence of the other three peaks observed in the recoil spectrum against the D^o. In particular there is some evidence for

$$e^+e^- \rightarrow D^{*+}D^{*-} , \qquad (5)$$

$$\text{or} \qquad \rightarrow D^+D^{**-} \text{ and charge conjugate ,} \qquad (5')$$

only much weaker relative to reaction (4). This feature is clearer if we compare the recoil spectra for "fixed" masses at E_{cm} = 4.028 GeV. In Fig. 11 we show these recoil spectra for the $(K\pi)^o$, $(K3\pi)^o$ and $(K\pi\pi \text{ exotic})^{\pm}$ signals each with the appropriate background subtraction.

IV. MASSES, WIDTHS AND MASS DIFFERENCES

For mass determination we focus on a single energy: E_{cm} = 4.028 GeV. We can then consider momentum distributions p of the two-particle system. In Fig. 12a we show the momentum spectrum for $K^{\mp}\pi^{\pm}$, together with the kinematic reflections "$\pi^+\pi^-$" and "$K\bar{K}$", in 10 MeV intervals. In Fig. 12b the same for the $K^{\mp}\pi^{\pm}\pi^{\pm}$ system. The background level is sketeched in on these.

In Fig. 13a and 13b we show these same distributions in 20 MeV intervals, with background subtracted.

A. Momentum Values

Several peaks stand out prominently:

$$p_1 = 765 \pm 12 \text{ MeV/c},$$

$$p_2 = 560 \pm 8 \text{ MeV/c}$$

with a "satellite structure" ~ 50 MeV/c lower,

$$p_3 = 178 \pm 8 \text{ MeV/c}, \quad \Gamma_3 = 35 \pm 8 \text{ MeV/c}$$

for the neutral distributions and

$$p_4 = 535 \pm 10 \text{ MeV/c}$$

for the charged distribution. Here the indices correspond to the reactions quoted above. The errors are estimates of the precision to which the central values are known including an allowance for systematic errors in the momentum scale. Finally the incident energy is

$$E_{cm}/2 = E_o = 2014 \pm 2.7 \text{ MeV} .$$

Here the error has three components added in quadrature: ± 2 MeV from the 0.1% uncertainty in the absolute energy calibration, ± 1.4 MeV beam spread from synchrotron radiation effects, and ± 1 MeV variation (which is known from flip coil measurements) in precise run-to-run beam settings. As far as widths of distributions are concerned the latter two errors contribute in quadrature giving $dE_o = 1.7$ MeV.

B. D^{*o} Decay

The possibilities for D^{*o} decay with charm conservation are:

$$D^{*o} \rightarrow D^o + \pi^o \qquad (6)$$

$$D^{*o} \rightarrow D^o + \gamma \ . \qquad (7)$$

The Q value for π^o production is so small that we can ask which of these two decay modes is the predominant one. Here $Q_{\pi^o} = M_{D^{*o}} - M_{D^o} - m_{\pi^o}$. We also note that the $D^{*o} \rightarrow D^+ \pi^-$ decay will be ruled out by energy conservation.

In Figs. 14a,b we show momentum spectra resulting from Monte-Carlo calculations for reactions (2) and (3) with D^{*o} decays according to (6) and (7) respectively. These were calculated at $E_{cm} = 4028$ MeV and for M_{Do} and $M_{D^{*o}}$ values as indicated. It is clear that the shape of the peak centered at p_3 is a sensitive function of whether we are dealing with π^o or γ decay of D^{*o}. For π^o decay (Fig. 14a) we get an essentially Gaussian distribution while for γ decay (Fig. 14b) we get a distribution with $dN/dp^2 =$ constant or $dN/dp \propto p$. It can be noted from a comparison of Fig. 12a with Fig. 14 that the predominant decay mode is π^o decay; however

there is evidence for appreciable γ decay as well. A preliminary estimate for $\Gamma(D^{*o} \to D^o\gamma)/\Gamma(D^{*o} \to D^o\gamma \text{ and } D^o\pi^o)$ is $\sim 35-45\%$.

C. Mass Determinations

We can quote the following preliminary values. From reaction (1) using p_1 we get a mass estimate for M_{Do} from $M_{Do}^2 = E_o^2 - p_1^2$

$$M_{Do}(1) = 1863 \pm 5.3 \text{ MeV}/c^2 \ .$$

Here the error is arrived at from $dM_{Do}(1) = 1.1\, dE_o - 0.4\, dp_1$. From reaction (2) using p_2 we get a relation between M_{Do} and M_{D*o} from $2E_o = E_{Do} + E_{D*o}$. In a linear approximation this is given by:

$$M_{Do}(2) + M_{D*o} = 3869 \pm 6.4 \text{ MeV} \ .$$

Here the error is arrived at from

$$dM_{Do}(2) = 2.1\, dE_o - 0.6\, dp_2 - dM_{D*o} \ .$$

From reaction (3) we get

$$M_{D*o}^2 = E_o^2 - \left(p_3 \frac{M_{D*o}}{M_{Do}}\right)^2 \ .$$

This gives:

$$\boxed{M_{D*o} = 2005 \pm 3 \text{ MeV}/c^2}$$

where the error comes from

$$dM_{D*o}(3) = dE_o - 0.1\, dp_3 \ .$$

Using this M_{D*o} value in the relation for $M_{Do}(2)$ we get

$$\boxed{M_{Do} = 1864 \pm 5.4 \text{ MeV}/c^2} \ .$$

Here $dM_{Do}(2,3) = 1.1\, dE_o - 0.6\, dp_2 + 0.1\, dp_3$.

The resulting value for $Q_{\pi o}$ is

$$Q_{\pi o} = 6 \pm 5.1 \text{ MeV}$$

where the error comes from $dQ_{\pi o} = 0.6\, dp_2 - 0.2\, dp_3$ since the dependence on dE_o (essentially) cancels here.

The experimental width Γ_3 is a very sensitive function of $Q_{\pi o}$. In particular the observed width Γ_3 fits best with a $Q_{\pi o}$ even lower than 6 MeV. Aside from the experimental resolution the contributions to the width Γ_3 come from $Q_{\pi o}$, Γ_{Do}, Γ_{D*o}, and $dE_o = 1.7$ MeV (the portion

contributing to the broadening of the distribution). This places more stringent limits on Γ_{D^o} and $\Gamma_{D^{*o}}$ of < 5 MeV. From charm theory Γ_{D^o} is expected to be $\ll 1$ eV (weak decay) while $\Gamma_{D^{*o}}$ is of typical electromagnetic width because of the very low Q_{π^o} value.

Finally from reaction (4) and p_4 we get a relation between M_{D^+} and $M_{D^{*+}}$ which in a linear approximation becomes:

$$M_{D^+} + M_{D^{*+}} = 3883 \pm 7.3 \text{ MeV} \quad .$$

Here the error is arrived at from:

$$dM_{D^+}(4) = 2.1\, dE_o - 0.6\, dp_4 - dM_{D^{*+}} \quad .$$

This yields $(M_{D^+} + M_{D^{*+}}) - (M_{D^o} + M_{D^{*o}}) = 14 \pm 7.7$ MeV/c^2, where now the error in E_o cancels. We have no reliable experimental determination for δ and δ^* where we define $\delta = M_{D^+} - M_{D^o}$ and $\delta^* = M_{D^{*+}} - M_{D^{*o}}$. Here $\delta + \delta^* = 14 \pm 7.7$ MeV/c^2. If from theory δ and δ^* are considered approximately equal[7,8,9] we get

$$\delta \approx \delta^* \approx 7 \pm 4 \text{ MeV}/c^2 \quad .$$

If on the other hand as suggested by Ono[10] $\delta \approx \delta^* + 3$ MeV/c^2,

$$\delta \approx 8.5 \pm 4 \text{ MeV}/c^2$$

and $$\delta^* \approx 5.5 \pm 4 \text{ MeV}/c^2 \quad .$$

As shown in Fig. 11c we have an indication for reaction (5); this gives an upper limit on $M_{D^{*+}}$, namely E_o; i.e.,

$$M_{D^{*+}} < 2014 \text{ MeV}/c^2 \quad .$$

This limit is consistent with the δ^* values quoted above.

D. Does p_3 Correspond to $D^{*o}D^{*o}$ or D^oD^{**o}?

With the value for $M_{D^{*o}}$ given above $Q = E_{cm} - 2M_{D^{*o}} = 18$ MeV, and $p(D^{*o}) = 191$ MeV/c. This represents a phenomenal rise from threshold for reaction (3), a p-wave process. In fact it has been suggested[11] that perhaps process (3'), with D^{**o} a $J^P = 1^+$ state with mass $M(D^{**o}) = 2146$ MeV/c^2 and s-wave production, could be occurring. From a very preliminary study of the M_{recoil} spectrum at $E_{cm} = 4.415$ GeV we find however no evidence for a recoil mass peak near 2146 MeV/c^2 but find

instead a braod peak at $M_{recoil} \approx 2200\ MeV/c^2$ and $\Gamma \approx 80\ MeV/c^2$. These values are completely consistent with values expected from reaction (3).

E. Study of an Individual Event

We have studied individual events to try and find examples of "complete" events; viz.,

$$e^+e^- \rightarrow \overline{D^o} \quad D^{*o}$$
$$\overline{D^o} \rightarrow K^+\pi^- , \quad D^{*o} \rightarrow D^o\pi^o , \quad D^o \rightarrow K^-\pi^+ \quad .$$

We have observed one clear-cut case at $E_{cm} = 4028$ MeV (see Fig. 15). This event gives a good fit to the above assumption and has been further constrained by a hand calculation to demand equal masses for the D^o and $\overline{D^o}$. This gives

$$M_{D^o} = 1866.5\ MeV/c^2$$
$$M_{D^{*o}} = 2006.7\ MeV/c^2 \quad .$$

The event does not fit a missing γ-ray.

This result lies well within the errors of the mass determinations given above. Figure 16 shows a sketch of the (central values) of the relations between M_{D^o}, $M_{D^{*o}}$, M_{D^+}, $M_{D^{*+}}$, δ and δ^* as well as the above event.

V. THE τ-θ PUZZLE REVISITED; EVIDENCE FOR PARITY VIOLATION FROM $D^{\pm}$ DECAY

A study of the $D^{\pm} \rightarrow K\pi\pi$ Dalitz plot shows that the plot is compatible with a phase space distribution, does not appear to die off on the boundaries as a natural spin parity assignment would, and is specifically incompatible with J^P assignments of 1^- or 2^+. These observations, coupled with the observation of the $K\pi$ decay of the D^o, a final state of natural spin parity ($J^P = 0^+, 1^-, 2^+, \ldots$), and the belief that the neutral and charged particles are members of the same isomultiplet, suggest parity violation in the decay of the D's.

A. Appearance of Dalitz Plot

In order to obtain a relatively clean sample of the decay $D^{\pm} \rightarrow K^{\mp}\pi^{\pm}\pi^{\pm}$

we apply mass and missing mass cuts to three-body combinations for data taken between $3.9 < E_{cm} < 4.25$ GeV. The cuts are $1860 < M_{K\pi} < 1920$ MeV/c^2 and $1960 < M_{recoil} < 2040$ MeV/c^2 (see Fig. 17). From this selection we obtain a sample of 126 events of which we estimate 58 events to be background. In Fig. 18a we present the Dalitz plot for these 126 events, choosing the Dalitz variables:

$$X_{Dalitz} = \frac{\left|T_{\pi_1} - T_{\pi_2}\right|}{\sqrt{3}\,Q} \; ; \quad Y_{Dalitz} = \frac{T_K}{Q}$$

with T being D rest frame kinetic energies and $Q = T_{\pi_1} + T_{\pi_2} + T_K$. Figure 18b shows a background Dalitz plot consisting of non-exotic $K\pi\pi$ combinations, $K^{\pm}\pi^{+}\pi^{-}$, with identical kinematic cuts. Both the signal and background plots appear uniformly populated without either boundary zeros or zeros along the y axis as expected for natural spin parity assignment. In order to specifically rule out the states 1^- and 2^+ we have performed Monte-Carlo simulations using the simple, phenomenological matrix elements presented by Zemach.[12]

B. The 1^- Matrix Element

For the case of $J^P = 1^-$ we construct an axial vector amplitude symmetric under the exchange of the two pions. A simple representation is provided by: $(T_{\pi_1} - T_{\pi_2})(\vec{\pi}_1 \times \vec{\pi}_2)$ where $\vec{\pi}$ represents a D rest frame pion momentum. For the case of unpolarized production one then expects an intensity proportional to $|T_{\pi_1} - T_{\pi_2}|^2 |\vec{\pi}_1 \times \vec{\pi}_2|^2$.

For comparison with the data we have divided the Dalitz plot into the four discrimination regions[13] of Fig. 19a. These regions are nearly evenly populated by phase space whereas the 1^- matrix element strongly populates region 3 at the expense of regions 1 and 4. Figure 20a compares the background subtracted region populations of the data to the populations expected in the 1^- model, both distributions normalized to the phase space Monte Carlo.

C. The 2^+ Matrix Element

Again following Zemach[12] we construct a symmetric, traceless second-rank tensor which is also symmetric under the exchange of the two pions. A simple example is provided by: $A^{ij} = \Delta\pi^i q^j + \Delta\pi^j q^i$ where $\vec{\Delta\pi}$ is the difference of the pion momenta and $\vec{q}$ is their cross product.

For unpolarized production one expects intensity proportional to

$$\sum_i \sum_j A^{ij} A_{ji} \quad \text{or} \quad |\vec{\pi}_1 - \vec{\pi}_2|^2 |\vec{\pi}_1 \times \vec{\pi}_2|^2 \ .$$

The discrimination regions for the 2^+ matrix elements are shown in Fig. 19b. Comparison of the region populations to the data is shown in Fig. 20b.

The χ^2 comparison between phase space and the respective 1^- and 2^+ matrix elements are given on Fig. 20.

We have thus demonstrated from a study of the $K\pi\pi$ Dalitz plot that this three-body final state is incompatible with J^P assignments of either 1^- or 2^+. $J^P = 0^+$ is not an allowed state of three pseudoscalars. Since the presumed isomultiplet state, D^o, decays into two pseudoscalars, a final state of natural spin parity, we conclude there exists evidence for parity violation in the decays of the D's, which implies that we are dealing with a weak decay.

VI. THE PRODUCT OF CROSS SECTION AND BRANCHING RATIO

We have searched for the charmed particle signal at all the energies from the ψ/J up to $E_{cm} = 7.8$ GeV. I have already shown in Figs. 2 and 3 the absence of any D^o signal in the $K^{\mp}\pi^{\pm}$ decay mode at the ψ and ψ'. Above $E_{cm} \sim 3.9$ GeV where we begin to observe a D^o signal the cross section rises rapidly to a maximum value of $\sigma \cdot BR = 0.6 \pm 0.1$ nb (preliminary) for the $K^{\mp}\pi^{\pm}$ decay mode at $E_{cm} = 4.028$ GeV. This is followed by a rapid drop off by a factor of ~ 3 at 4.4 GeV. Beyond 4.6 GeV the cross section drops off further to a level where we either cannot observe a signal at all or can just barely recognize it. The preliminary $\sigma \cdot BR$ distribution is shown in Fig. 21. To obtain $BR(K^{\mp}\pi^{\pm})$ one needs to

study "complete" events like the one illustrated in Fig. 15. This study is in progress. As "complete" events are very rare, this indicates that $BR(K^{\mp}\pi^{\mp})$ is small, of the order of a few percent.

$\sigma \cdot BR(K^{\mp}\pi^{\pm}\pi^{\pm}) \approx 0.3 \pm 0.15$ nb at $E_{cm} = 4.028$ GeV, evaluation at other energies is in progress. Finally $\sigma \cdot BR(K3\pi)$ is approximately 2 to 3 times larger than $\sigma \cdot BR(K^{\mp}\pi^{\pm})$ but the detailed study is not complete as yet.

VII. SEARCH FOR A CABIBBO FORBIDDEN DECAY MODE

According to charm theory[4] the decay $D^{o} \to K^{-}\pi^{+}$ proceeds with a $BR \propto \cos^{2}\theta$ while the decay $D^{o} \to \pi^{-}\pi^{+}$ proceeds with a $BR \propto \sin^{2}\theta$ where θ is the Cabibbo angle. We have searched for a $\pi^{-}\pi^{+}$ signal with optimal cuts on the recoil system. We find an indication at the 1.5 standard deviation level giving $BR(D^{o}(\overline{D^{o}}) \to \pi^{+}\pi^{-})/BR(D^{o}(\overline{D^{o}}) \to K^{\mp}\pi^{\pm}) = 6.5 \pm 4\%$ (see Fig. 22). Thus the effect is not established as yet.

The results presented here are the work of the LBL-SLAC collaboration at SPEAR, whose members are: F. M. Pierre, G. S. Abrams, M. S. Alam, A. M. Boyarski, M. Breidenbach, W. C. Carithers, W. Chinowsky, S. C. Cooper, R. G. DeVoe, J. M. Dorfan, G. J. Feldman, C. E. Friedberg, D. Fryberger, G. Hanson, J. Jaros, A. D. Johnson, J. A. Kadyk, R. R. Larsen, D. Lüke, V. Lüth, H. L. Lynch, R. J. Madaras, C. C. Morehouse, H. K. Nguyen, J. M. Paterson, M. L. Perl, I. Peruzzi, M. Piccolo, T. P. Pun, P. Rapidis, B. Richter, B. Sadoulet, R. H. Schindler, R. F. Schwitters, J. Siegrist, W. Tanenbaum, G. H. Trilling, F. Vannucci, J. S. Whitaker, and J. E. Wiss.

We wish to thank the SPEAR operating staff for their enthusiastic efforts in successfully carrying out the runs at 4.028 and 4.415 GeV under new conditions and very limited time. We also wish to thank the LBL and SLAC computer centers for their help in facilitating the data analysis. Finally I wish to thank Ms. Christina Frank for her meticulous work in typing and compiling this report.

REFERENCES AND FOOTNOTES

1. J.-E. Augustin et al., Phys. Rev. Lett. 34, 233 (1975); J.-E. Augustin et al., Phys. Rev. Lett. 34, 764 (1975).

2. G. Goldhaber, F. M. Pierre et al., Phys. Rev. Lett. 37, 255 (1976).

3. I. Peruzzi, M. Piccolo et al., Phys. Rev. Lett. 37, 569 (1976).

4. S. L. Glashow, J. Iliopoulos, and L. Maiani, Phys. Rev. D2, 1285 (1970); S. L. Glashow, Experimental Meson Spectroscopy, A.I.P. Conf. Proc. No. 21, Particles and Fields Subseries No. 8, p. 387 (1974). For more details, see also M. K. Gaillard, B. W. Lee, and J. L. Rosner, Rev. Mod. Phys. 47, 277 (1975); A. De Rujula, H. Georgi, and S. L. Glashow, Phys. Rev. D12, 147 (1975); M. B. Einhorn and C. Quigg, Phys. Rev. D12, 2015 (1975). Earlier indications of possible charmed particle production have come from experiments involving neutrino interactions, as well as from cosmic-ray emulsion studies. See, for example: A. Benvenuti et al., Phys. Rev. Lett. 34, 419 (1975); E. G. Cazzoli et al., Phys. Rev. Lett. 34, 1125 (1975); J. Blietschau et al., Phys. Lett. 60B, 207 (1976); J. von Krogh et al., Phys. Rev. Lett. 36, 710 (1976); B. C. Barish et al., Phys. Rev. Lett. 36, 939 (1976); K. Niu et al., Prog. Theor. Phys. 46, 1644 (1971).

5. See talks by D. Meyer and by P. Smusser for results from DESY presented at this topical conference.

6. For an alternate interpretation of the entire psion family, in terms of a color model, see G. Feldman and P. T. Mathews, The Discovery of Coloured Kaons?, Imperial College London Preprint ICTP/75/17, July 1976. Also a review by O. W. Greenberg and C. A. Nelson, Color Models of Hadrons, University of Maryland preprint PHYS.PUB.77-047.

7. A. De Rujula, H. Georgi, and S. L. Glashow, Phys. Rev. Lett. 37, 398 (1976); K. Lane and E. Eichten, Phys. Rev. Lett. 37, 477 (1976).

8. K. Lane and S. Weinberg, Phys. Rev. Lett. 37, 717 (1976). See also H. Fritzsch, Phys. Lett. 63B, 419 (1976).

9. D. B. Lichtenberg, Phys. Rev. D12, 3760 (1975).

10. S. Ono, Phys. Rev. Lett. 37, 655 (1976).

11. M. Suzuki, private communication. Also, J. Finkelstein and S. S. Pinsky, Columbia University preprint COO-1545-198.

12. C. Zemach, Phys. Rev. B133, 1201 (1964). See also B. Lee, C. Quigg, and J. Rosner, Tests for Weak Decays of Charmed Particle Candidates, Fermilab preprint 76/63 Thy.

13. The inner boundary of region 4 is a contour of constant (and small) $|\vec{\pi}_1 \times \vec{\pi}_2|$.

This work was done with support from the U.S. Energy Research and Development Administration.

FIGURE CAPTIONS

Fig. 1. The ratio $R = \sigma_{had}/\sigma_{\mu\mu}$. The distribution corresponds to the pre-May 1976 data sample. The location of the two new high-statistics points 4.028 and 4.415 is also indicated.

Fig. 2. A composite of the $K\pi$ mass distribution for the ψ/J region, the ψ' region and the $E_{cm} = 3.9 - 4.6$ GeV region (all data) as well as the $E_{cm} = 4.028$ GeV data separately.

Fig. 3. Detail of the $K\pi$ mass spectrum in the $M = 1500 - 2500$ MeV/c^2 region for the same data samples as in Fig. 2.

Fig. 4. The two-body mass distributions with $M_{recoil} > 1800$ MeV/c for all data. (a) $K^{\mp}\pi^{\pm}$, (b) "$\pi^+\pi^-$," (c) "K^+K^-" and insert (d) which shows the $K^{\mp}\pi^{\pm}$ distributions as obtained by the two TOF methods for the $E_{cm} = 4.028$ GeV data only.

Fig. 5. The $K^{\mp}\pi^{\pm}\pi^+\pi^-$ mass distribution for the $E_{cm} = 3.9 - 4.6$ GeV region (all data).

Fig. 6. Comparison of the exotic ($K^{\mp}\pi^{\pm}\pi^{\pm}$) and non-exotic $K^{\mp}\pi^+\pi^-$ mass distributions for all data.

Fig. 7. Scatter plot $M(K^{\mp}\pi^{\pm})$ versus M_{recoil} for the "4.1" GeV data $E_{cm} = 3.9 - 4.25$ GeV.

Fig. 8. Scatter plot $M(K^{\mp}\pi^{\pm}\pi^{\pm})$ versus M_{recoil}. Data sample as in Fig. 7.

Fig. 9. (a) M_{recoil} distribution for the $K^{\pm}\pi^{\mp}$ signal as measured. (b) M_{recoil} distribution for the $K^{\pm}\pi^{\mp}$ signal, as well as the kinematic reflection signals "$\pi^+\pi^-$" and "$\bar{K}K$," for fixed $M_{K\pi} = 1865$ MeV/c^2. Each distribution is background subtracted as discussed in the text. $E_{cm} = 3.9 - 4.6$ GeV all data.

Fig. 10. M_{recoil} distribution for the $K^{\mp}\pi^{\pm}\pi^{\pm}$ signal as measured. The background subtraction comes from the same mass cuts on the non-exotic $K\pi\pi$ channel.

Fig. 11. The recoil spectra at $E_{cm} = 4.028$ GeV against $(K\pi)^o$, $(K3\pi)^o$ and $(K\pi\pi \text{ exotic})^{\pm}$ for fixed masses with background subtraction.

Fig. 12. Momentum spectra at E_{cm} = 4.028 GeV in 10 MeV/c intervals. (a) Signals observed in the two-body systems $K^{\mp}\pi^{\pm}$ as well as kinematic reflections "$\pi^+\pi^-$," "K^+K^-." (b) For the signal observed in $K^{\mp}\pi^{\pm}\pi^{\pm}$. The dashed curves indicate background levels.

Fig. 13. The same spectra as in Fig. 12, now in 20 MeV/c intervals and with background subtraction.

Fig. 14. Momentum spectra from Monte-Carlo calculation simulating the detector at SPEAR. (a) $D^{*o} \rightarrow D^o + \pi^o$. (b) $D^{*o} \rightarrow D^o + \gamma$.

Fig. 15. Computer reconstruction of an example of $e^+e^- \rightarrow \overline{D^o}D^{*o}$, $\overline{D^o} \rightarrow K^+\pi^-$, $D^{*o} \rightarrow D^o\pi^o$, $D^o \rightarrow K^-\pi^+$. The right-hand part is an enlargement of the vertex region showing no measurable path length for D^o and $\overline{D^o}$ decay.

Fig. 16. Sketch of the relations between M_{Do} and M_{D*o}, M_{D+} and M_{D*+}. The π^oD^o, $\pi^oD^{\pm}$ and $\pi^{\pm}D^o$ thresholds are indicated by shading. The inset shows δ and δ^* as a function of M_{D*+} for the "best values" of M_{Do} = 1864 and M_{D*o} = 2005 MeV/c^2. For clarity the central values are only shown.

Fig. 17. The $K\pi\pi$ distribution for the "4.1" GeV region with an M_{recoil} cut 1960 - 2040 MeV/c^2. (a) Exotic, (b) non-exotic.

Fig. 18. Dalitz plots, folded around y-axis, for the $K\pi\pi$ system with mass cuts $M(K\pi\pi)$ = 1860 - 1920 MeV/c^2 and the selections given in Fig. 17. (a) Exotic, (b) non-exotic.

Fig. 19. The discrimination regions on the Dalitz plot selected for effective separation between phase space and (a) a 1^- matrix element, (b) a 2^+ matrix element.

Fig. 20. Comparison of background subtracted populations in the four discrimination regions (a) the 1^- model, (b) the 2^+ model, with all distributions normalized to phase space Monte-Carlo calculations. The respective χ^2 values and confidence levels are also shown.

Fig. 21. $\sigma \cdot BR$ for $K^{\mp}\pi^{\pm}(1865)$ production.

Fig. 22. $M(\pi^+\pi^-)$ distribution for the "4.1" GeV region with a cut of $M_{recoil} > 1800$ MeV/c^2. We note the kinematic reflection signal centered at 1740 MeV/c^2 as already shown in Fig. 4b, as well as a possible small excess of events consistent with 1865 MeV/c^2.

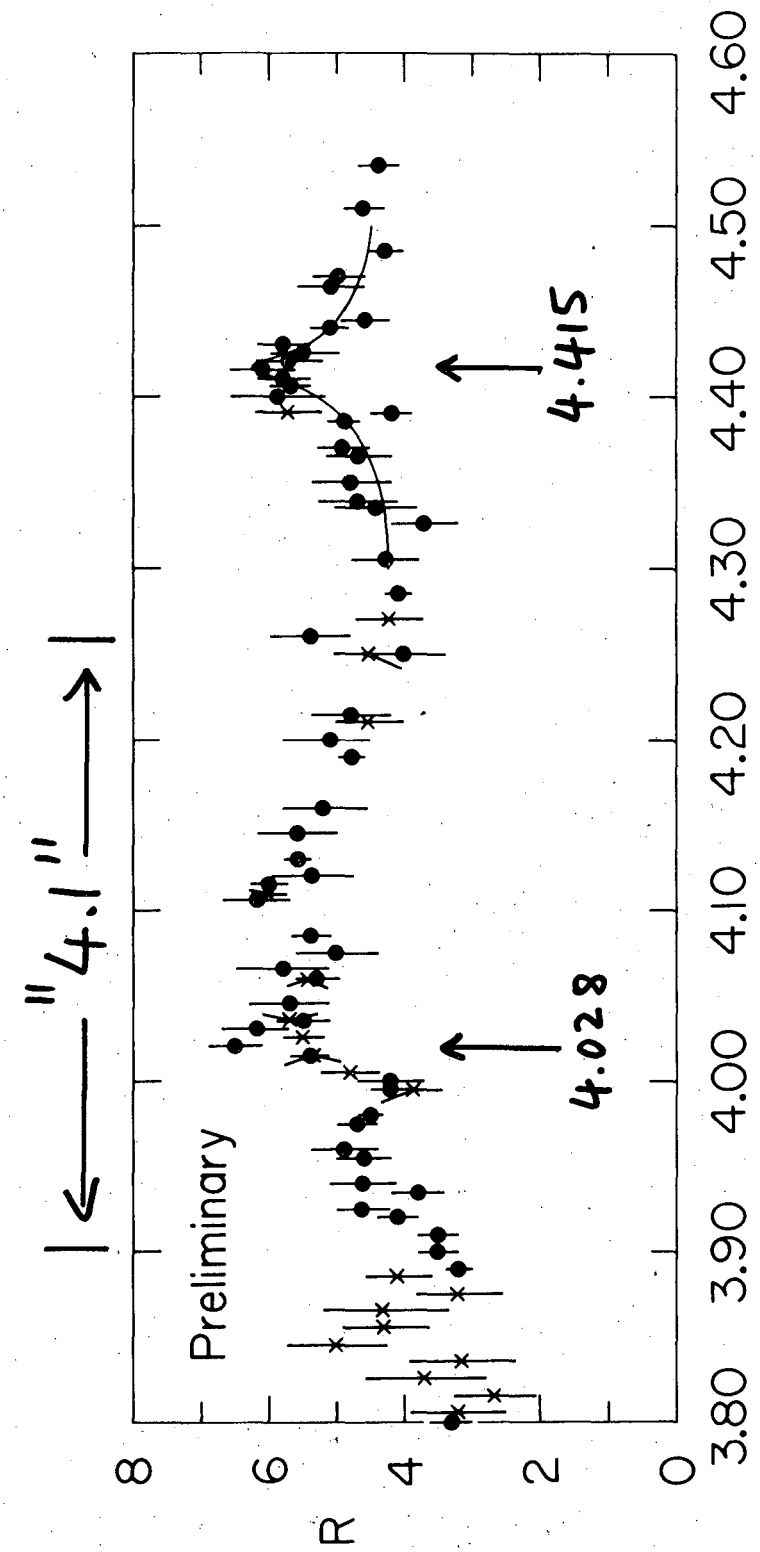

XBL 767-8808

Fig. 1

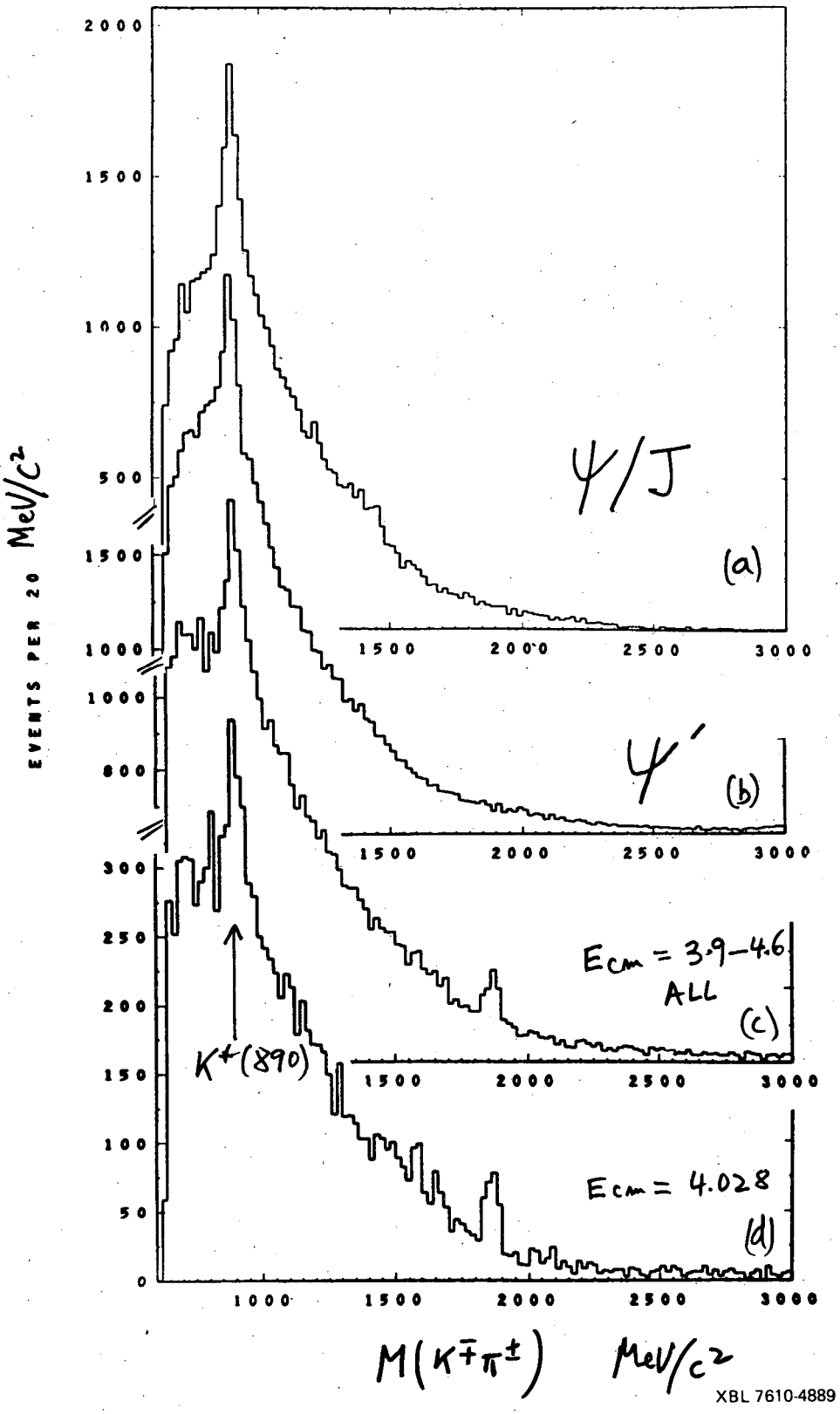
EVENTS PER 20 MeV/c²
ψ/J
(a)
ψ′
(b)
Ecm = 3.9–4.6
ALL
(c)
K±(890)
Ecm = 4.028
(d)
M(K∓π±) MeV/c²
XBL 7610-4889

Fig. 2

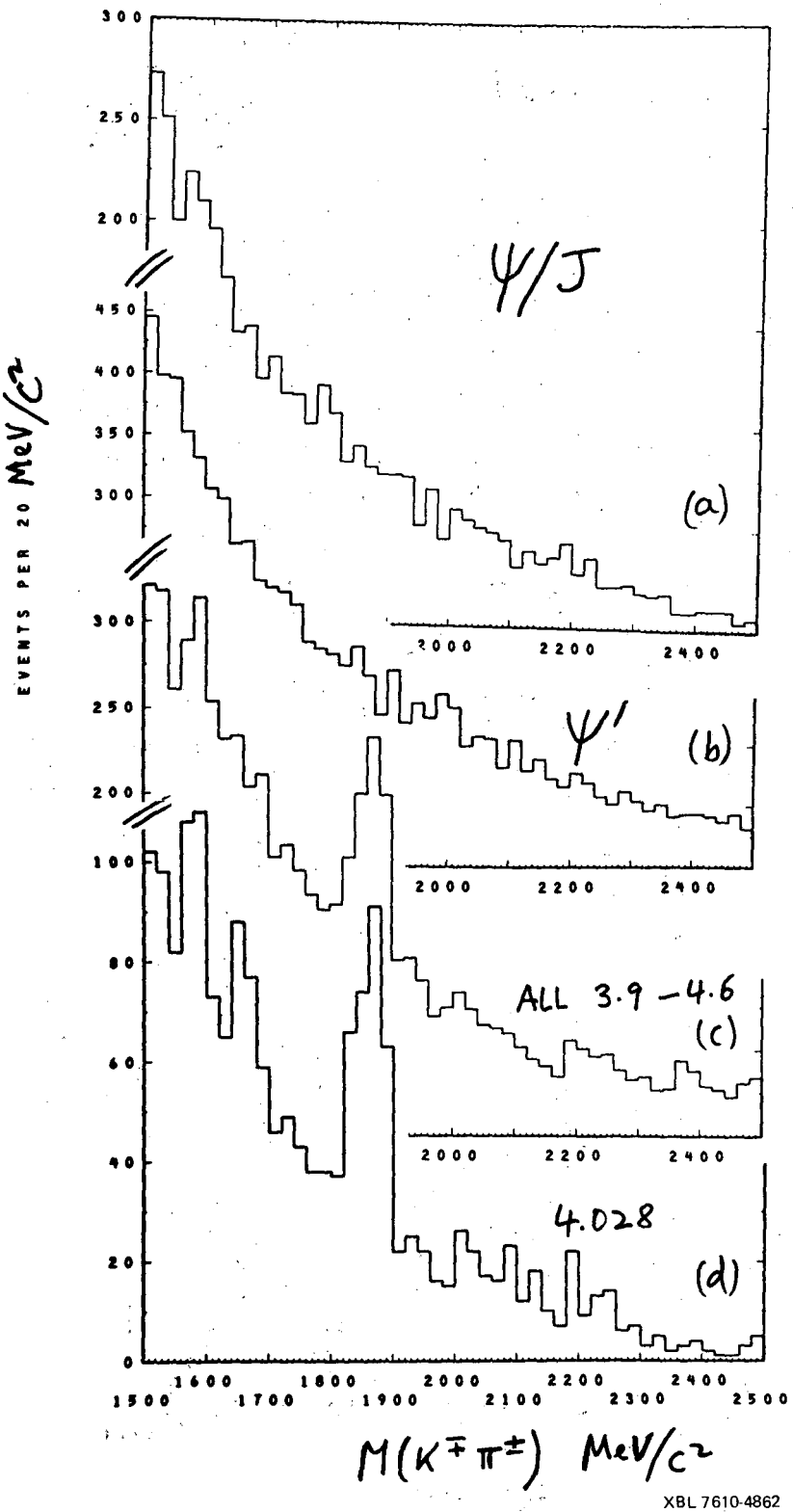
EVENTS PER 20 MeV/c²
ψ/J
(a)
ψ′
(b)
ALL 3.9 – 4.6
(c)
4.028
(d)
M(K∓π±) MeV/c²
XBL 7610-4862

Fig. 3

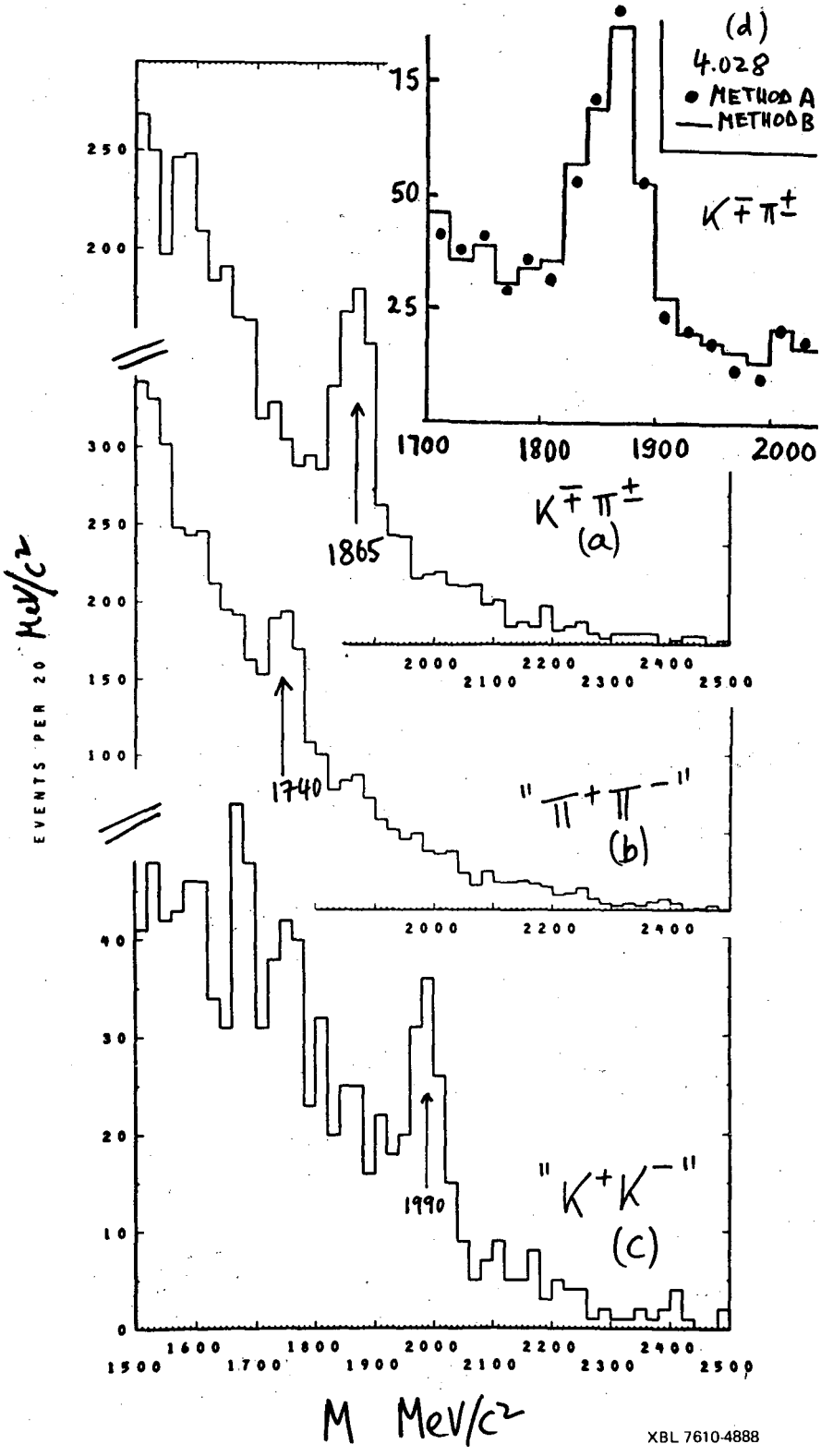
(d)
4.028
• METHOD A
— METHOD B
$K^{\mp}\pi^{\pm}$
1865
$K^{\mp}\pi^{\pm}$
(a)
1740
"$\pi^+\pi^-$"
(b)
1990
"K^+K^-"
(c)
EVENTS PER 20 MeV/c²
M MeV/c²
XBL 7610-4888

Fig. 4

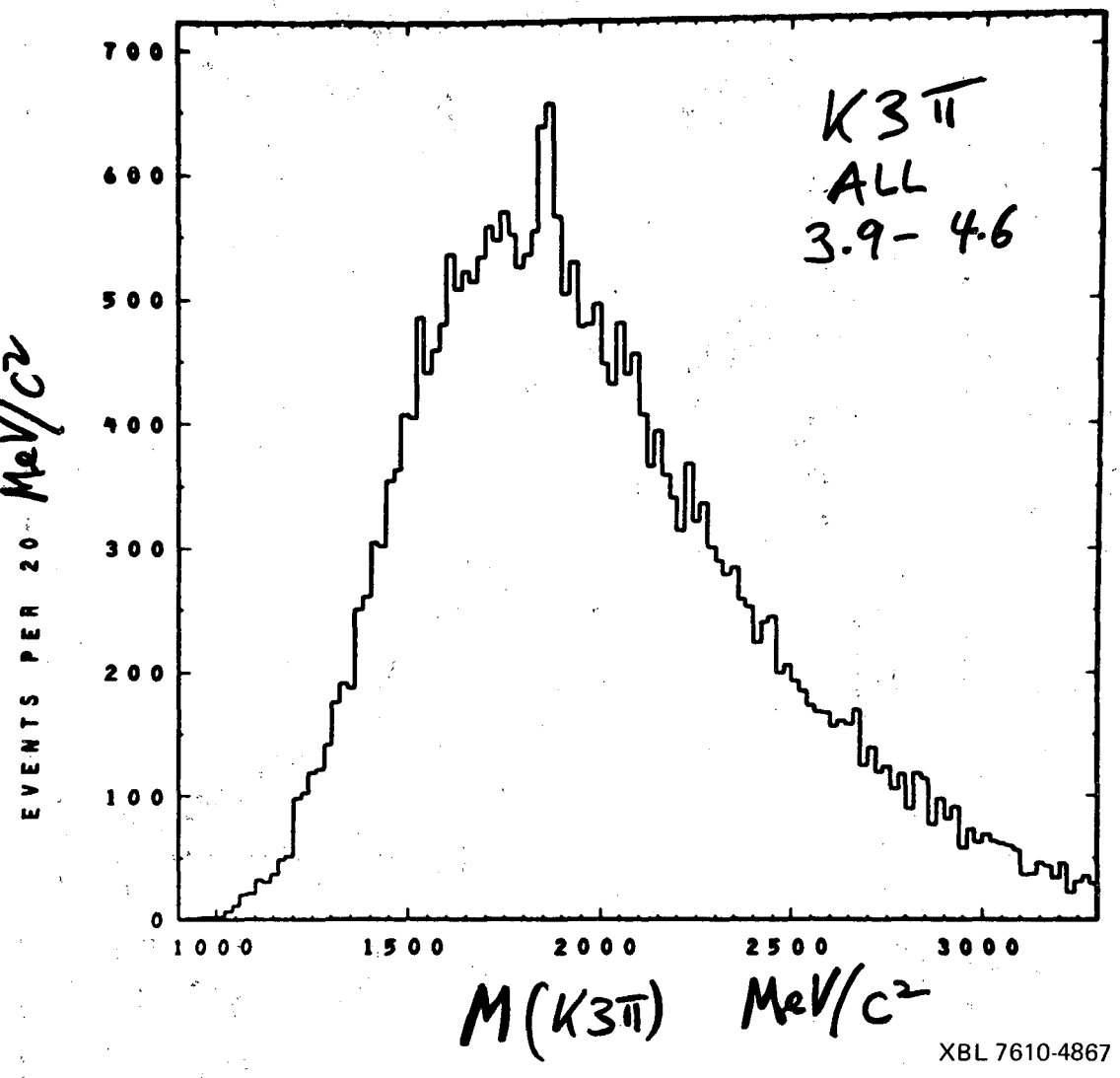

Fig. 5

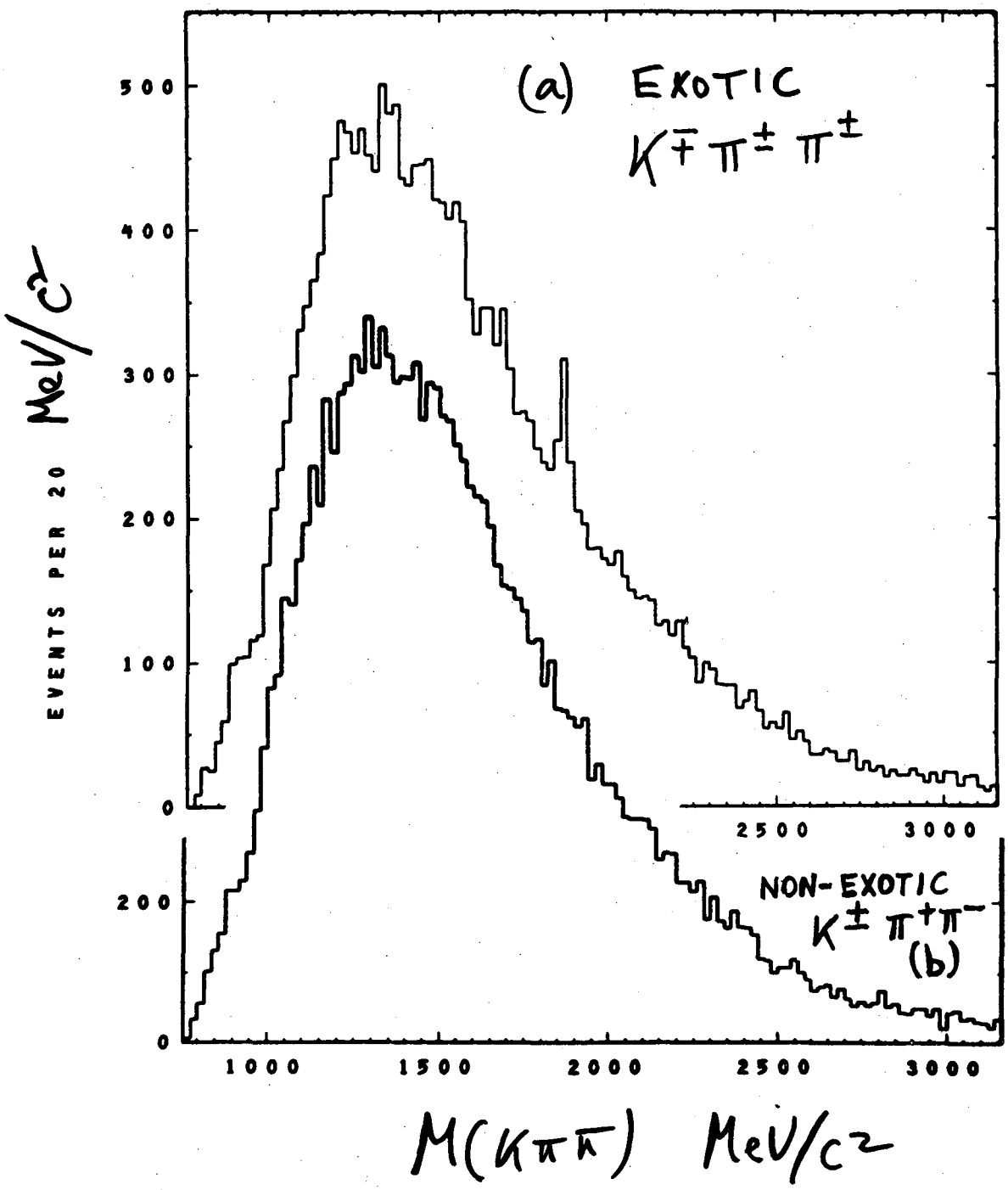
(a) EXOTIC
$K^{\mp}\pi^{\pm}\pi^{\pm}$
NON-EXOTIC
$K^{\pm}\pi^{+}\pi^{-}$
(b)
EVENTS PER 20 MeV/c²
M(Kππ) MeV/c²
500
400
300
200
100
0
200
0
1000
1500
2000
2500
3000
XBL 7610-4864

Fig. 6

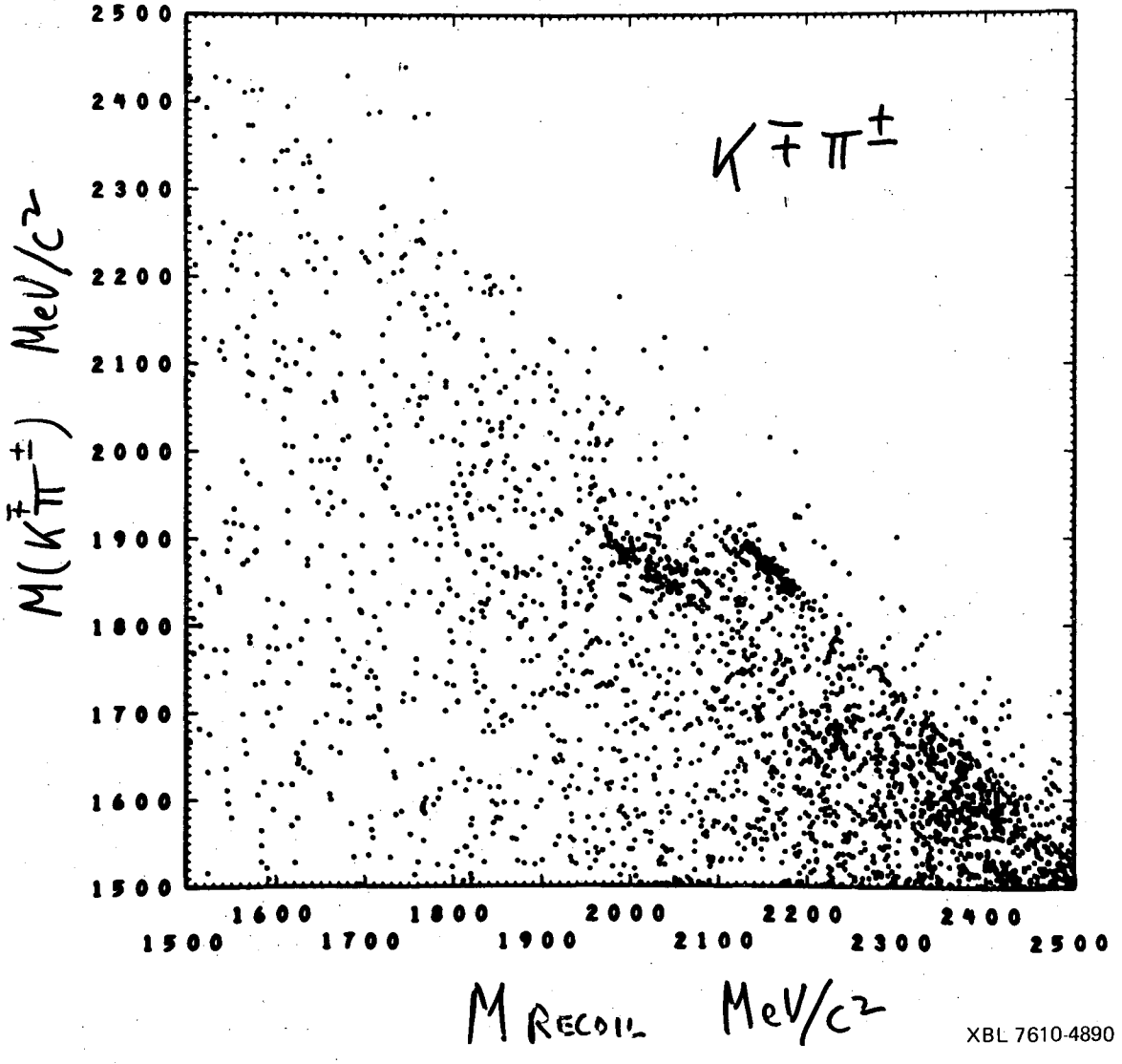

Fig. 7

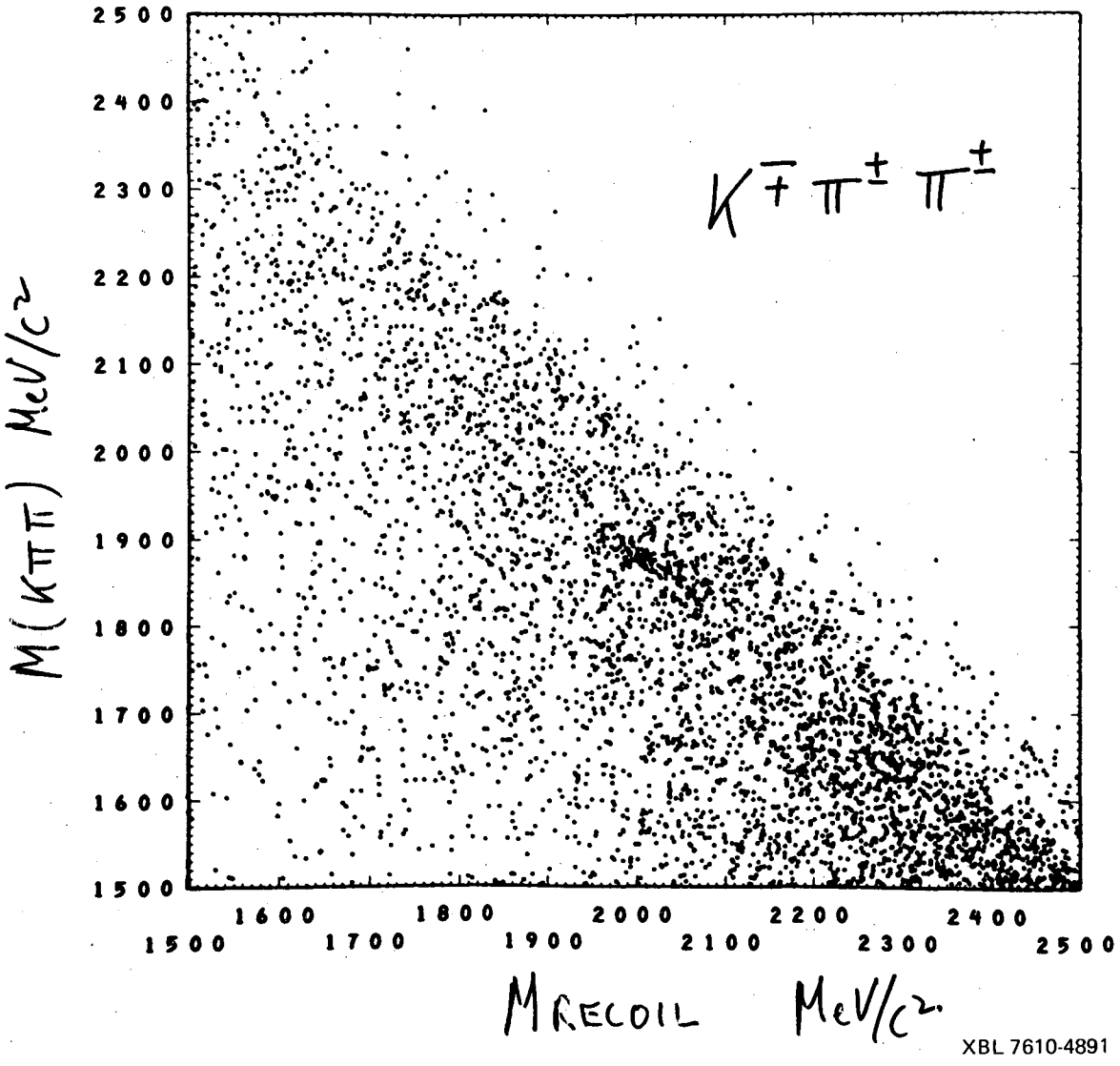
2500
2400
2300
2200
2100
2000
1900
1800
1700
1600
1500
M(KππΠ) MeV/c²
$K^{\mp}\pi^{\pm}\pi^{\pm}$
1500
1600
1700
1800
1900
2000
2100
2200
2300
2400
2500
M RECOIL MeV/c²
XBL 7610-4891

Fig. 8

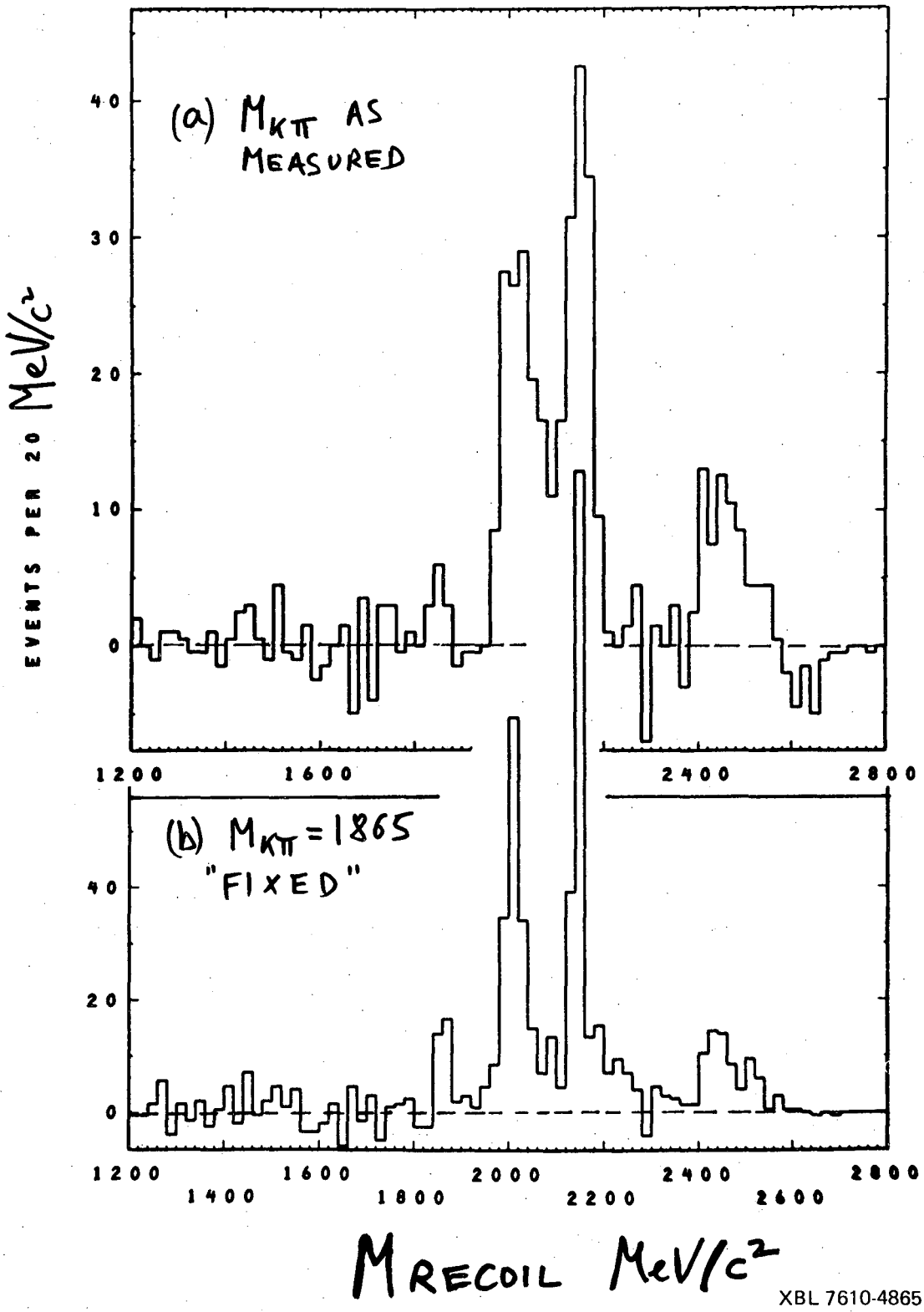

Fig. 9

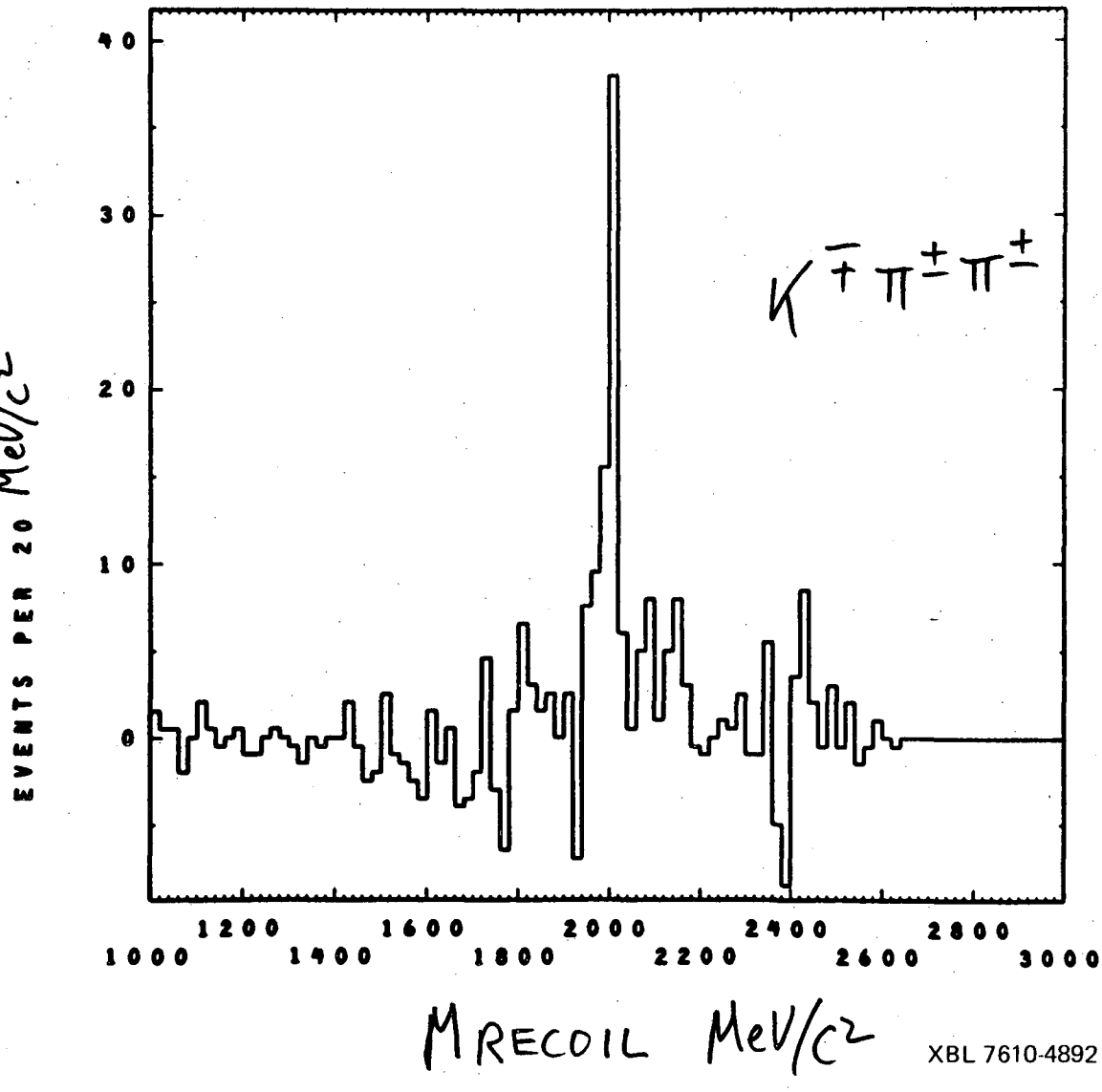
40
30
20
10
0
EVENTS PER 20 MeV/c²
1000
1200
1400
1600
1800
2000
2200
2400
2600
2800
3000
$K^{\mp}\pi^{\pm}\pi^{\pm}$
M RECOIL MeV/c²
XBL 7610-4892

Fig. 10

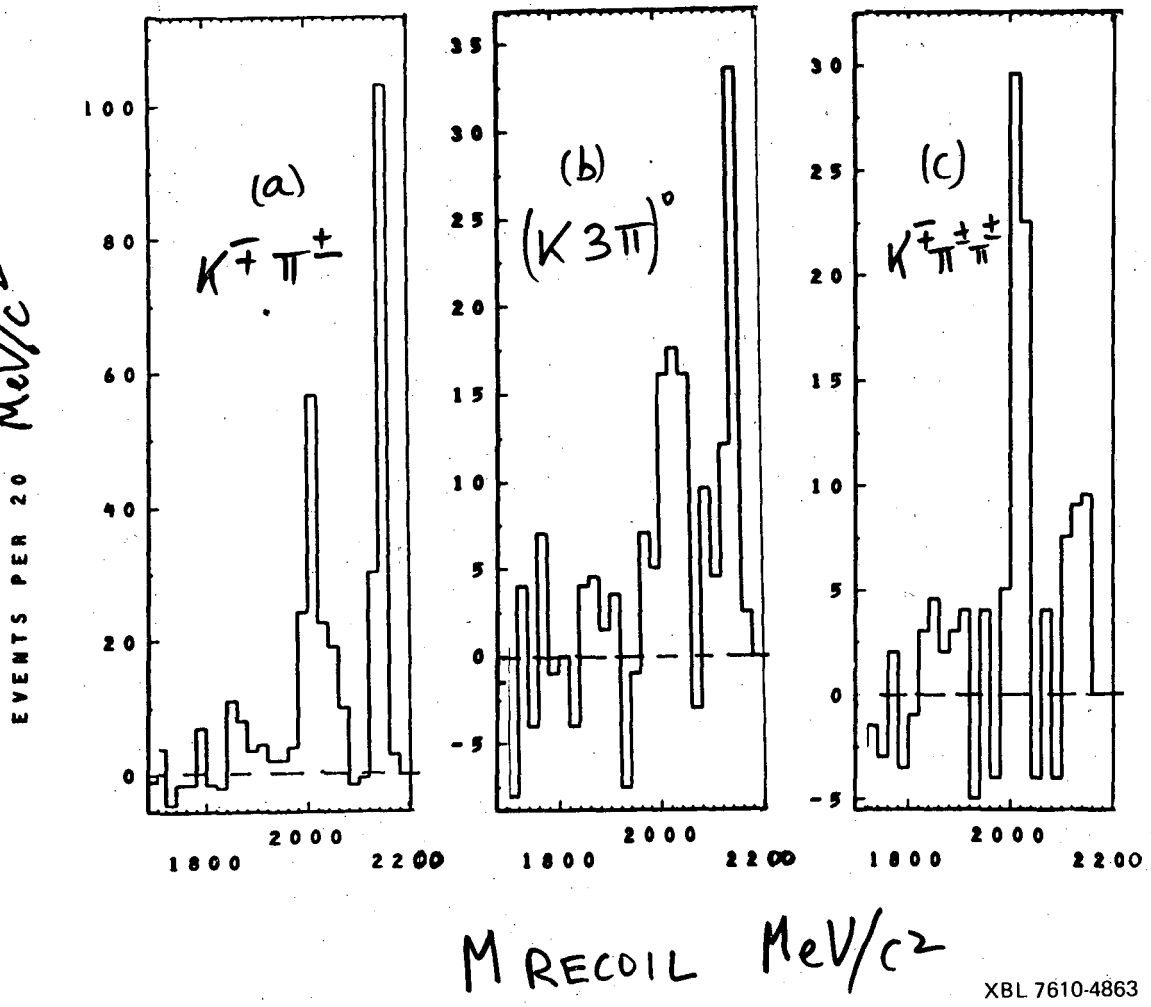

Fig. 11

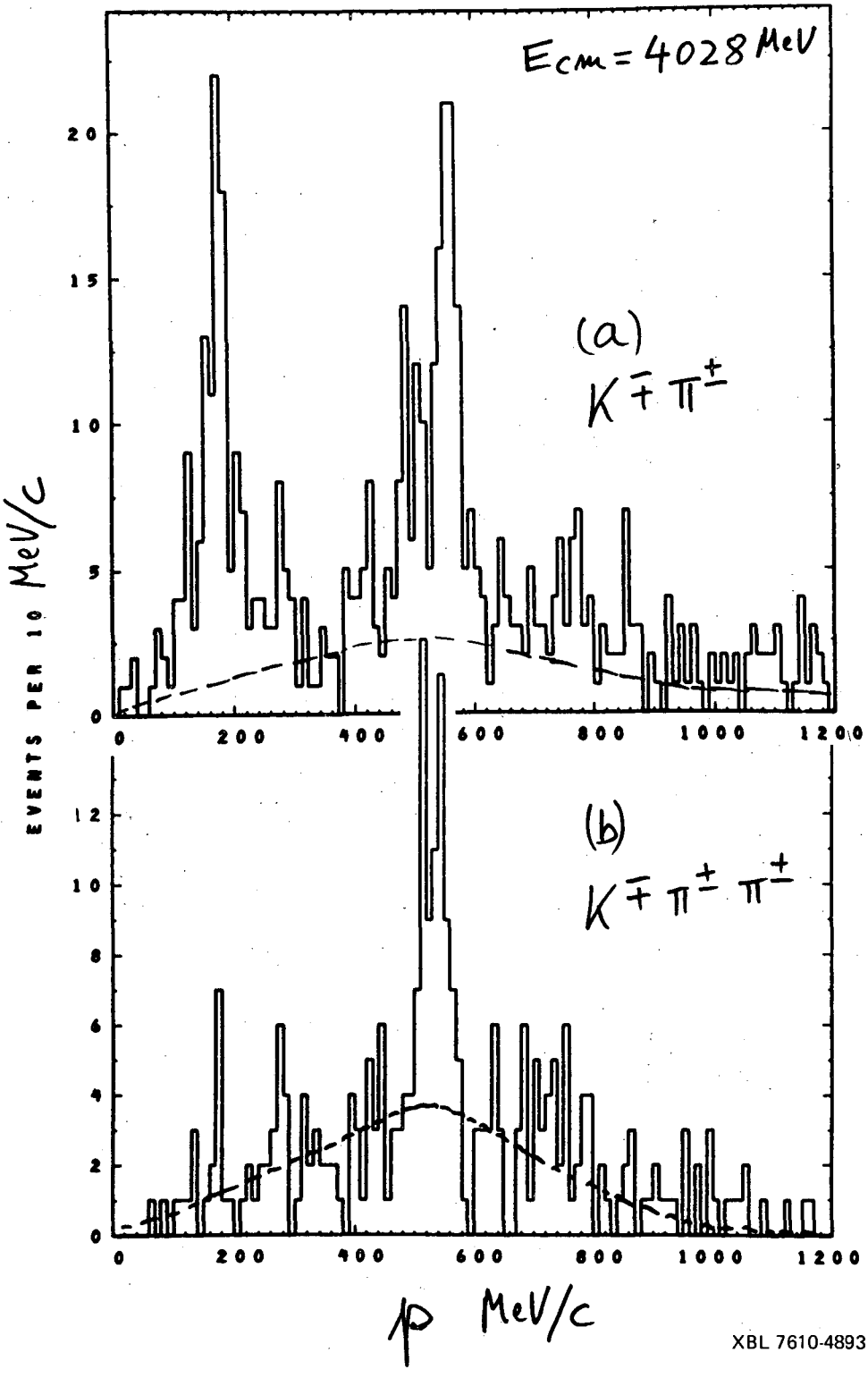
$E_{cm} = 4028$ MeV
(a)
$K^{\mp}\pi^{\pm}$
(b)
$K^{\mp}\pi^{\pm}\pi^{\pm}$
EVENTS PER 10 MeV/c
p MeV/c
0
200
400
600
800
1000
1200
XBL 7610-4893

Fig. 12

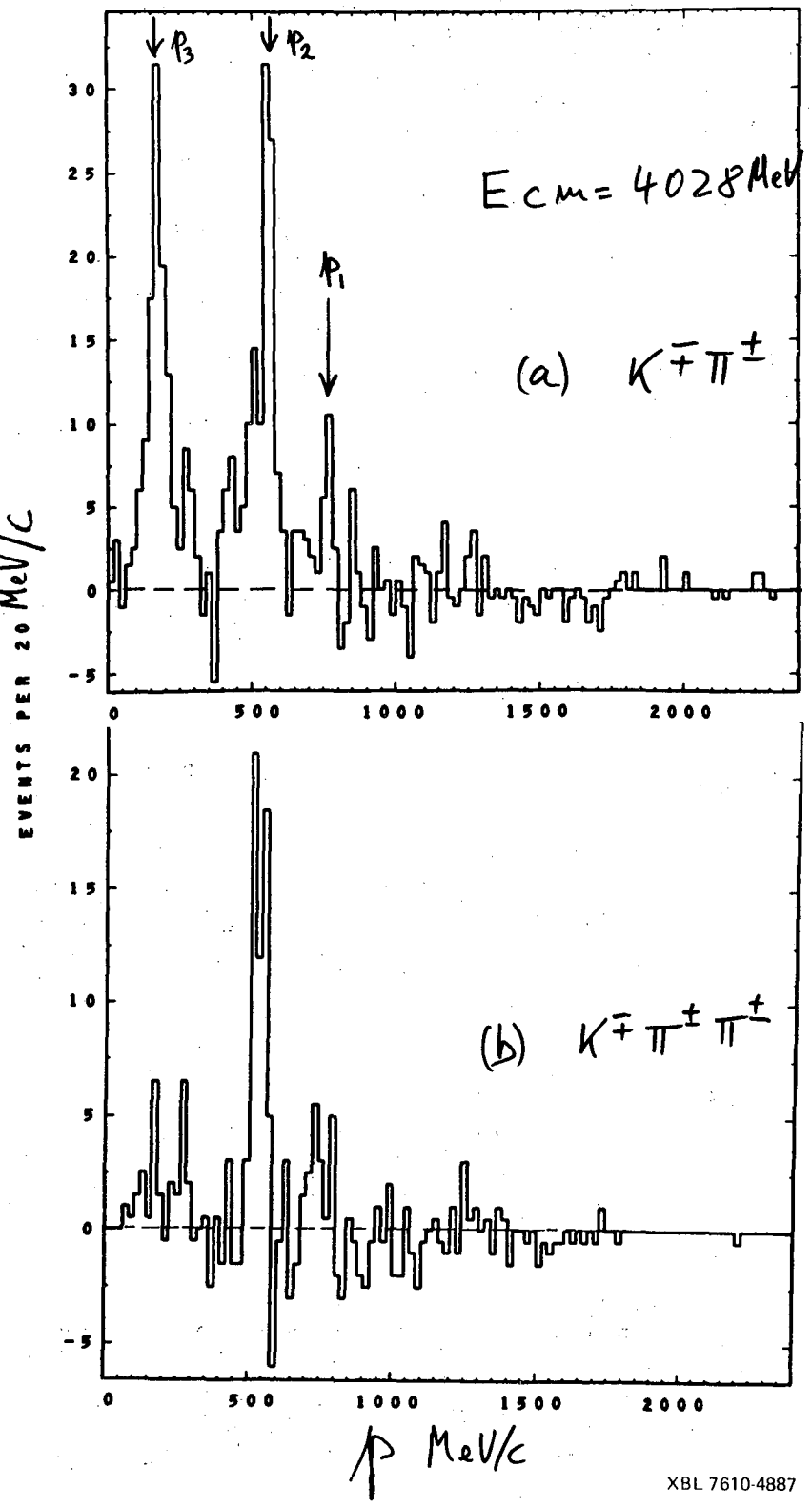

Fig. 13

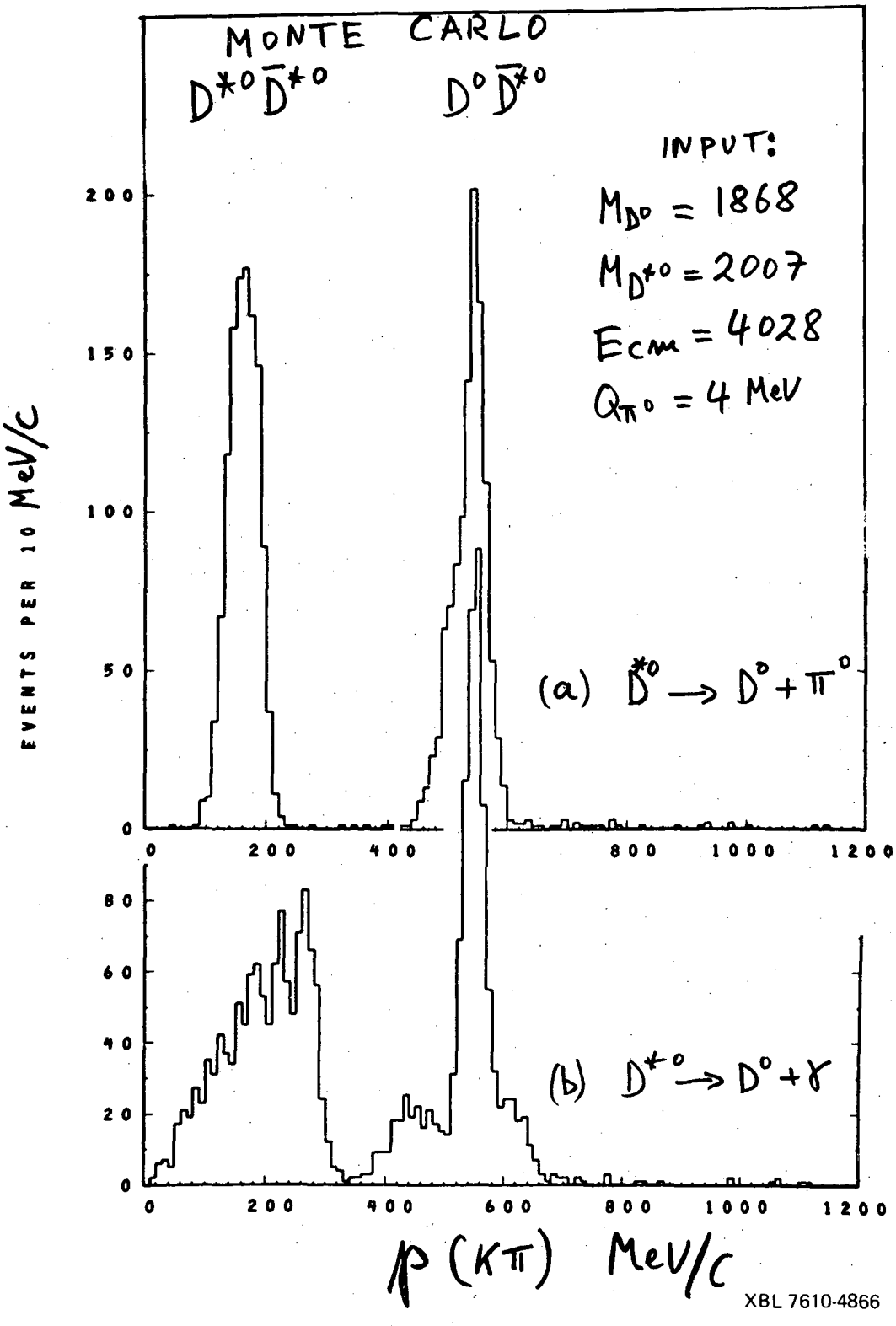
MONTE CARLO
D*0 D̄*0
D0 D̄*0
INPUT:
MD0 = 1868
MD*0 = 2007
Ecm = 4028
Qπ0 = 4 MeV
(a) D*0 → D0 + π0
(b) D*0 → D0 + γ
EVENTS PER 10 MeV/C
p (Kπ) MeV/c
XBL 7610-4866

Fig. 14

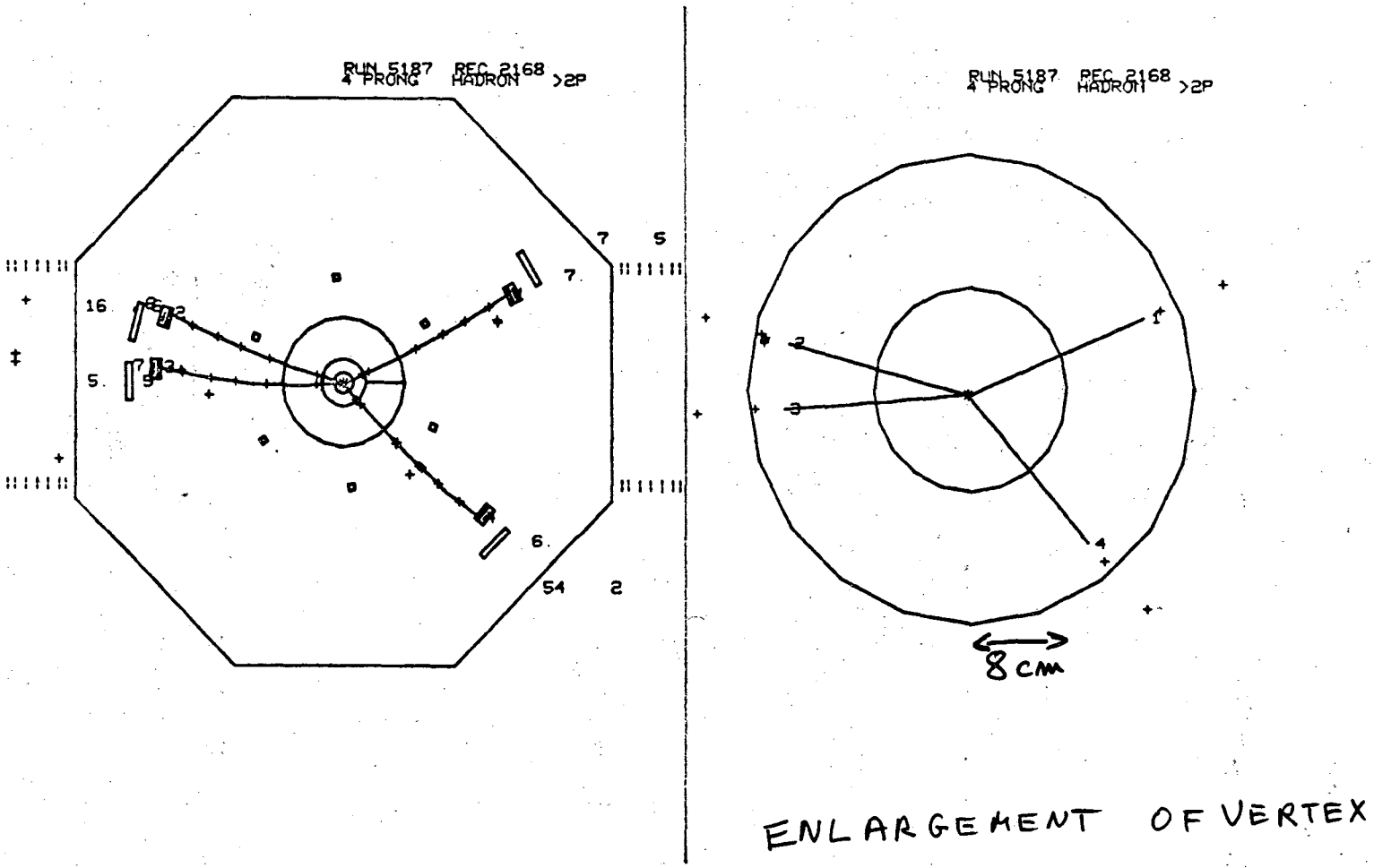

XBL 7610-4884

Fig. 15

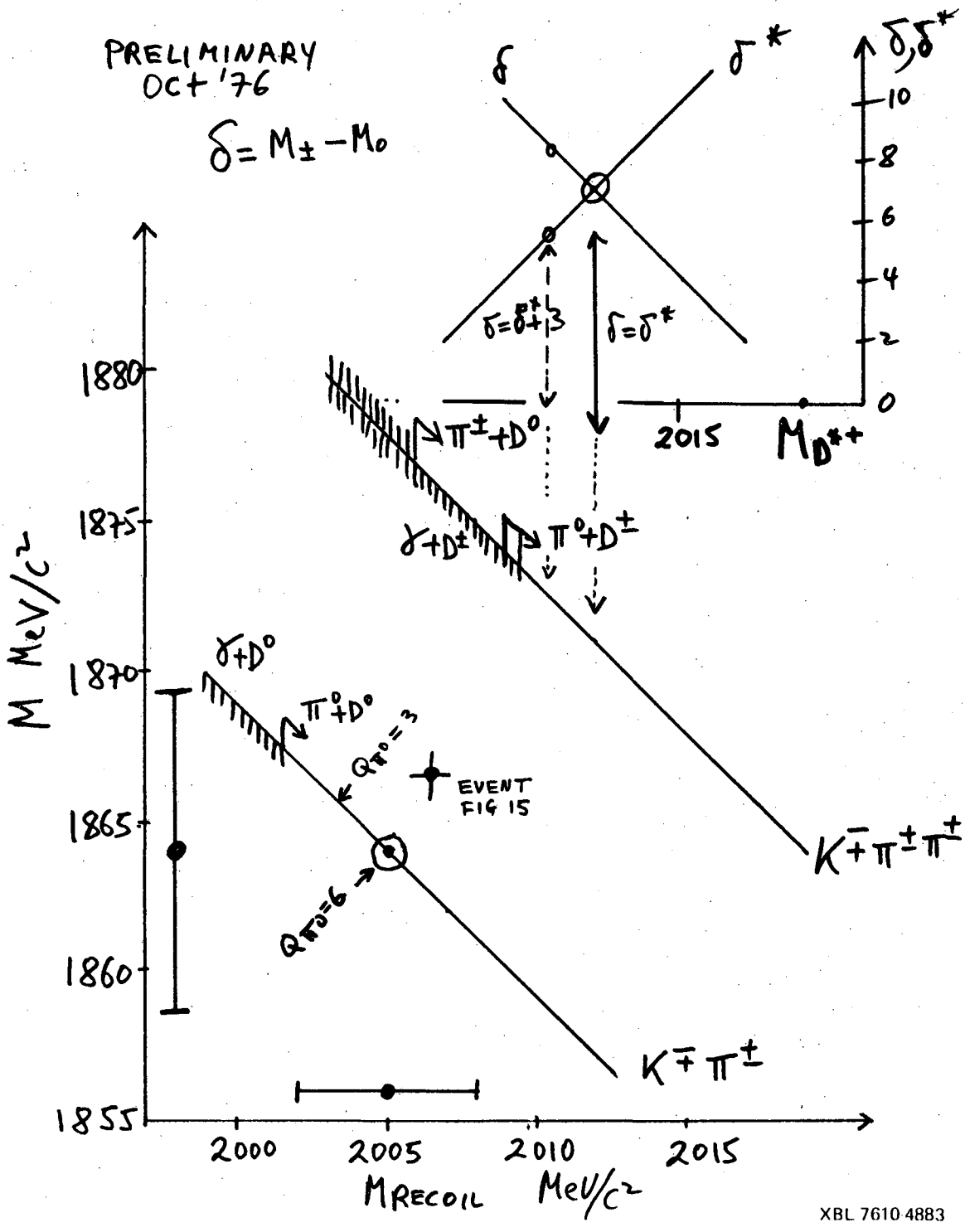
PRELIMINARY
OCT '76
$\delta = M_{\pm} - M_0$
δ
δ^*
δ, δ^*
10
8
6
4
2
0
$\delta = \delta^+ + 3$
$\delta = \delta^*$
$\pi^{\pm} + D^0$
2015
$M_{D^{*+}}$
$\gamma + D^{\pm}$
$\pi^0 + D^{\pm}$
$\gamma + D^0$
$\pi^0 + D^0$
$Q_{\pi^0} = 3$
EVENT
FIG 15
$Q_{\pi^0} = 6$
$K^{\mp}\pi^{\pm}\pi^{\pm}$
$K^{\mp}\pi^{\pm}$
1880
1875
1870
1865
1860
1855
M MeV/c^2
2000
2005
2010
2015
M_{RECOIL} MeV/c^2
XBL 7610 4883

Fig. 16

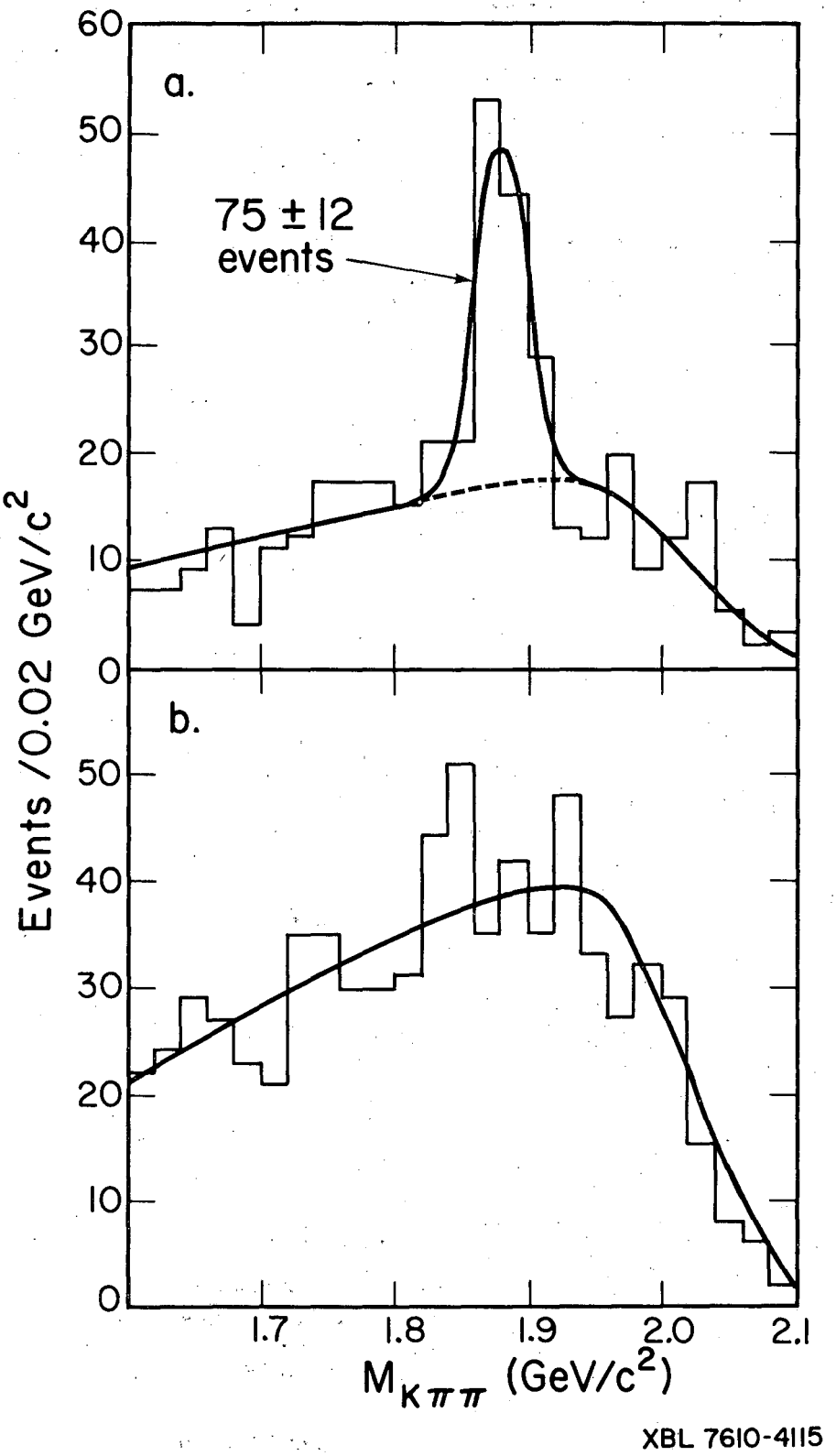

XBL 7610-4115

Fig. 17

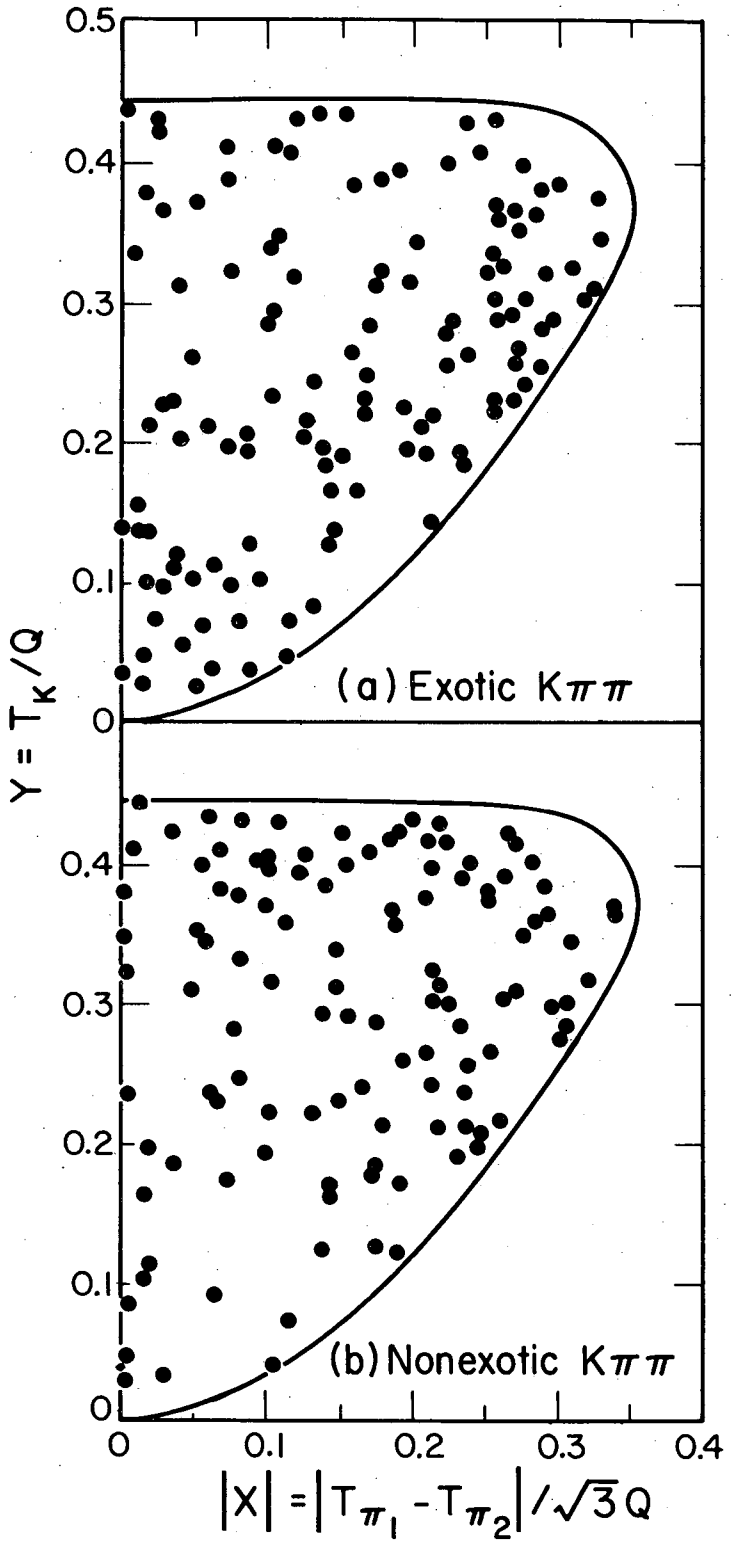

XBL 7610-4116

Fig. 18

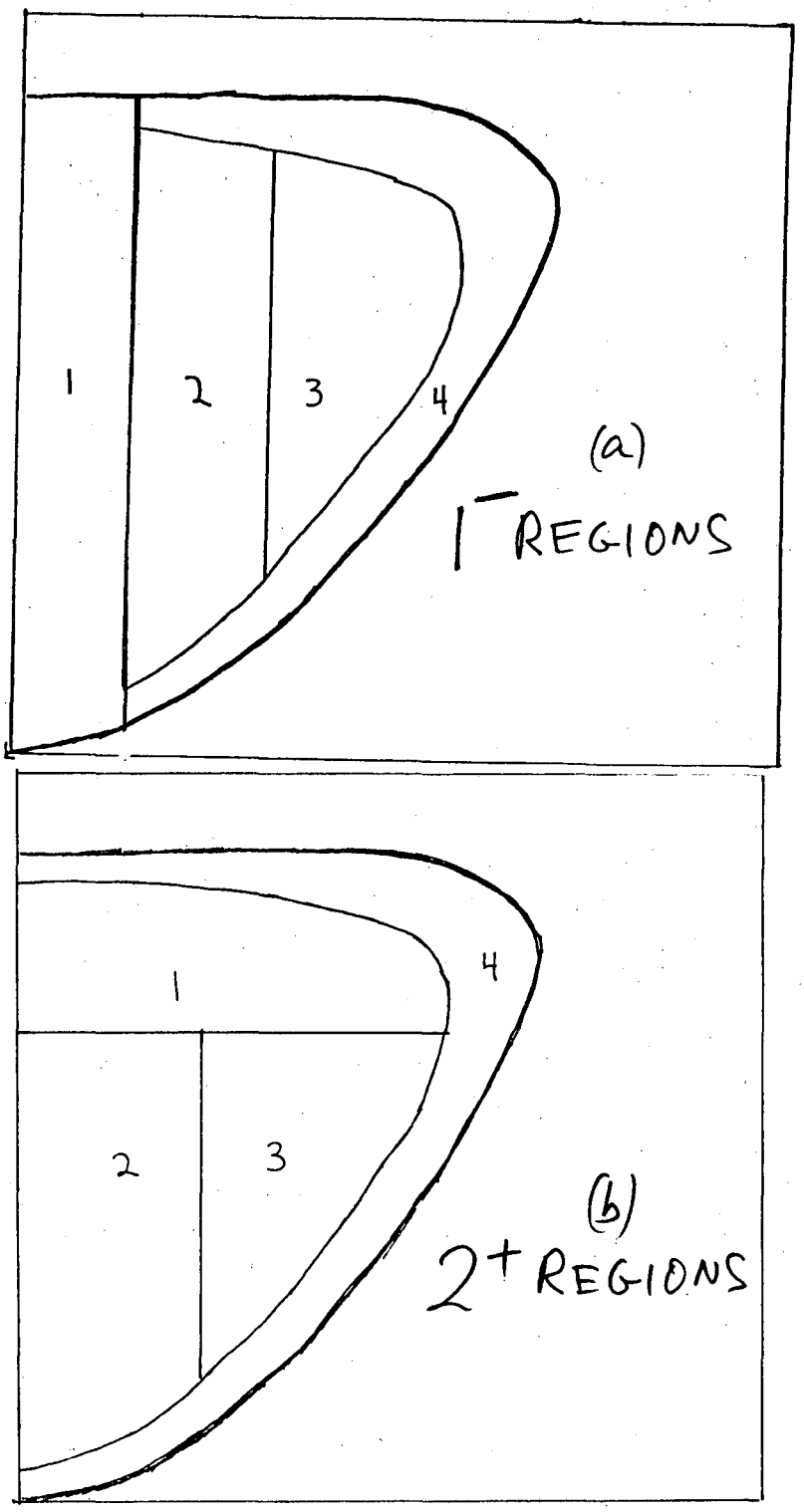

XBL 7610-4886

Fig. 19

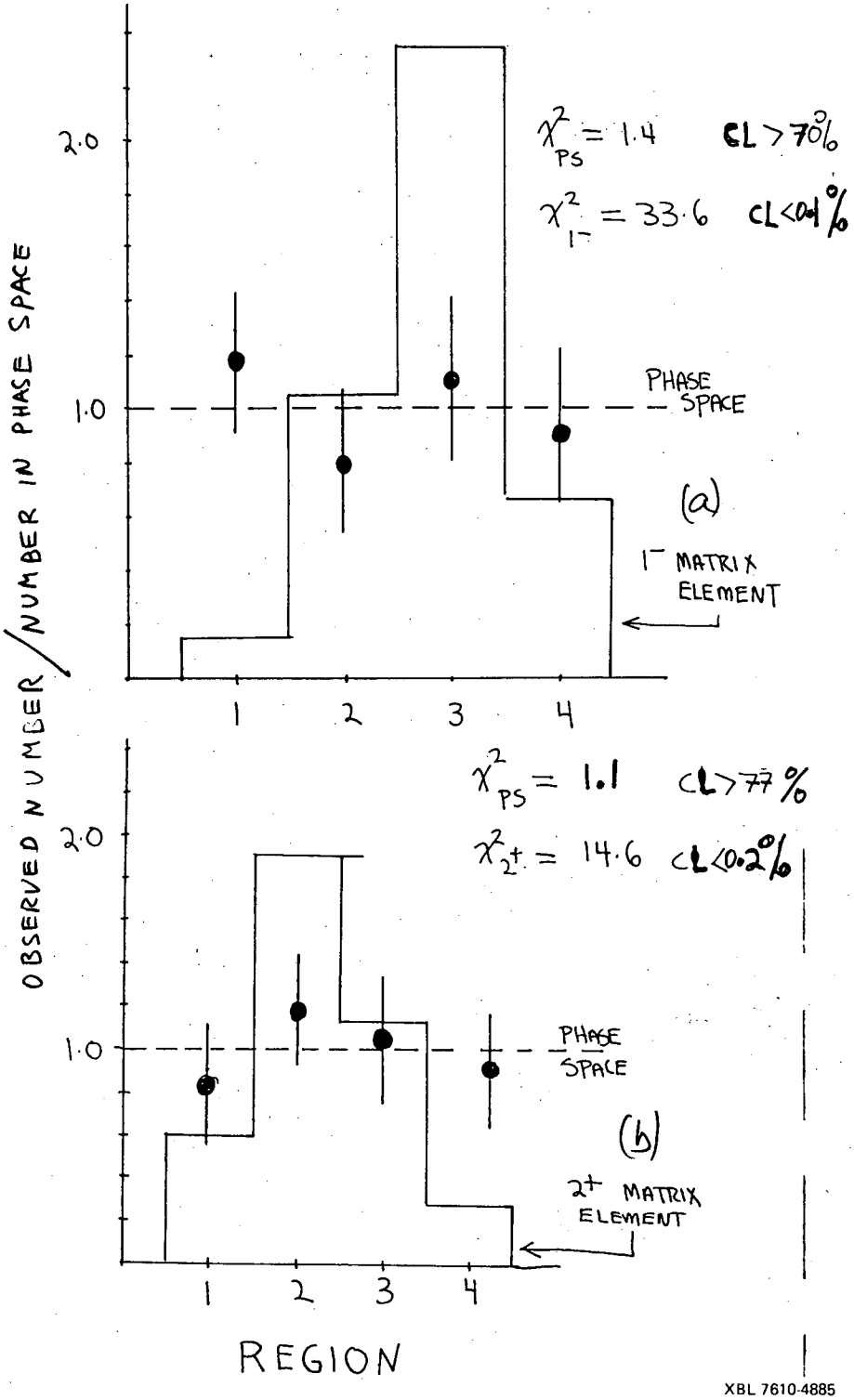
OBSERVED NUMBER / NUMBER IN PHASE SPACE
2.0
1.0
$\chi^2_{PS} = 1.4$ CL > 70%
$\chi^2_{1^-} = 33.6$ CL < 0.1%
PHASE SPACE
(a)
1⁻ MATRIX ELEMENT
1
2
3
4
$\chi^2_{PS} = 1.1$ CL > 77%
$\chi^2_{2^+} = 14.6$ CL < 0.2%
PHASE SPACE
(b)
2⁺ MATRIX ELEMENT
REGION
XBL 7610-4885

Fig. 20

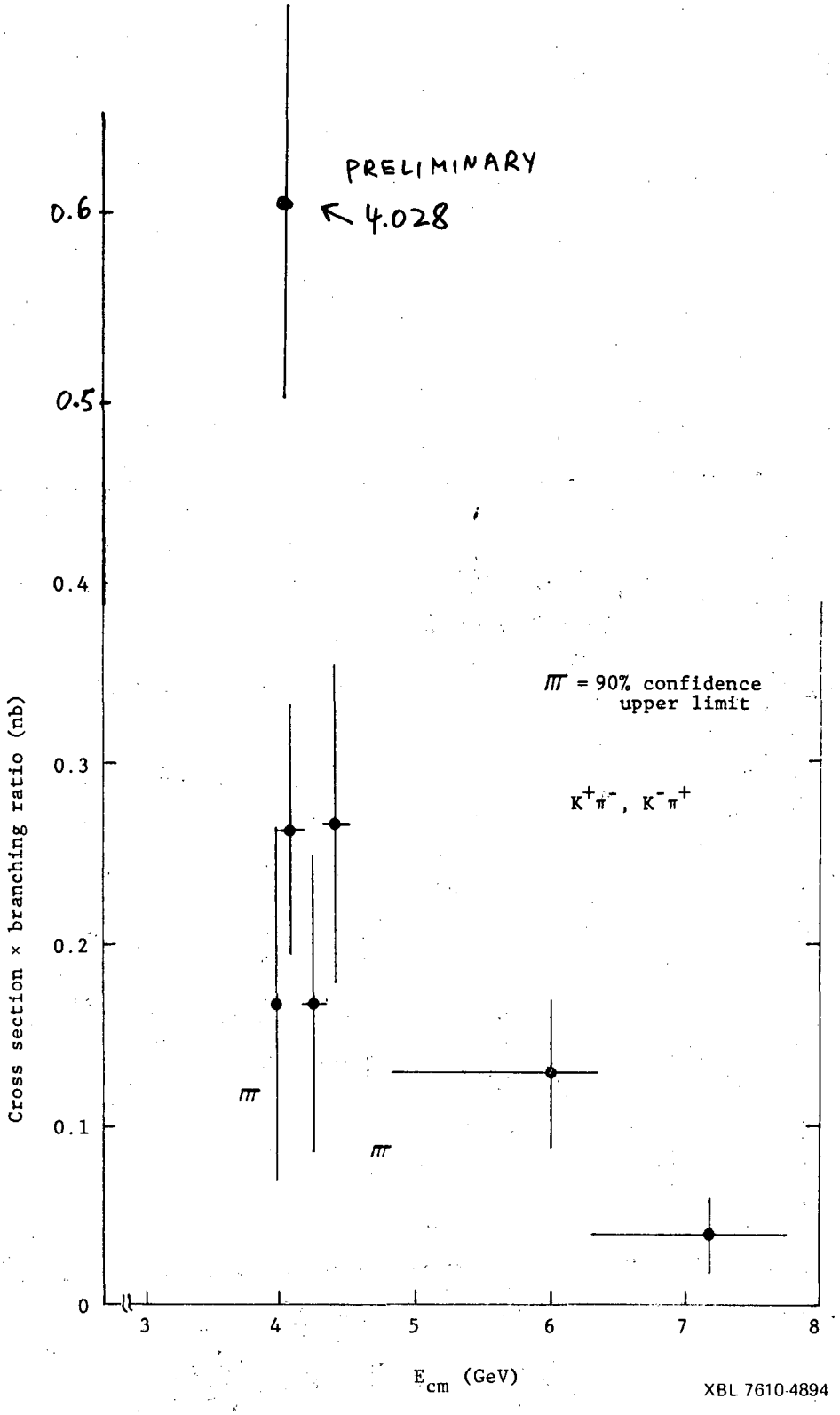
PRELIMINARY
4.028
0.6
0.5
0.4
0.3
0.2
0.1
0
Cross section × branching ratio (nb)
= 90% confidence upper limit
$K^+\pi^-$, $K^-\pi^+$
3
4
5
6
7
8
E_{cm} (GeV)
XBL 7610-4894

Fig. 21

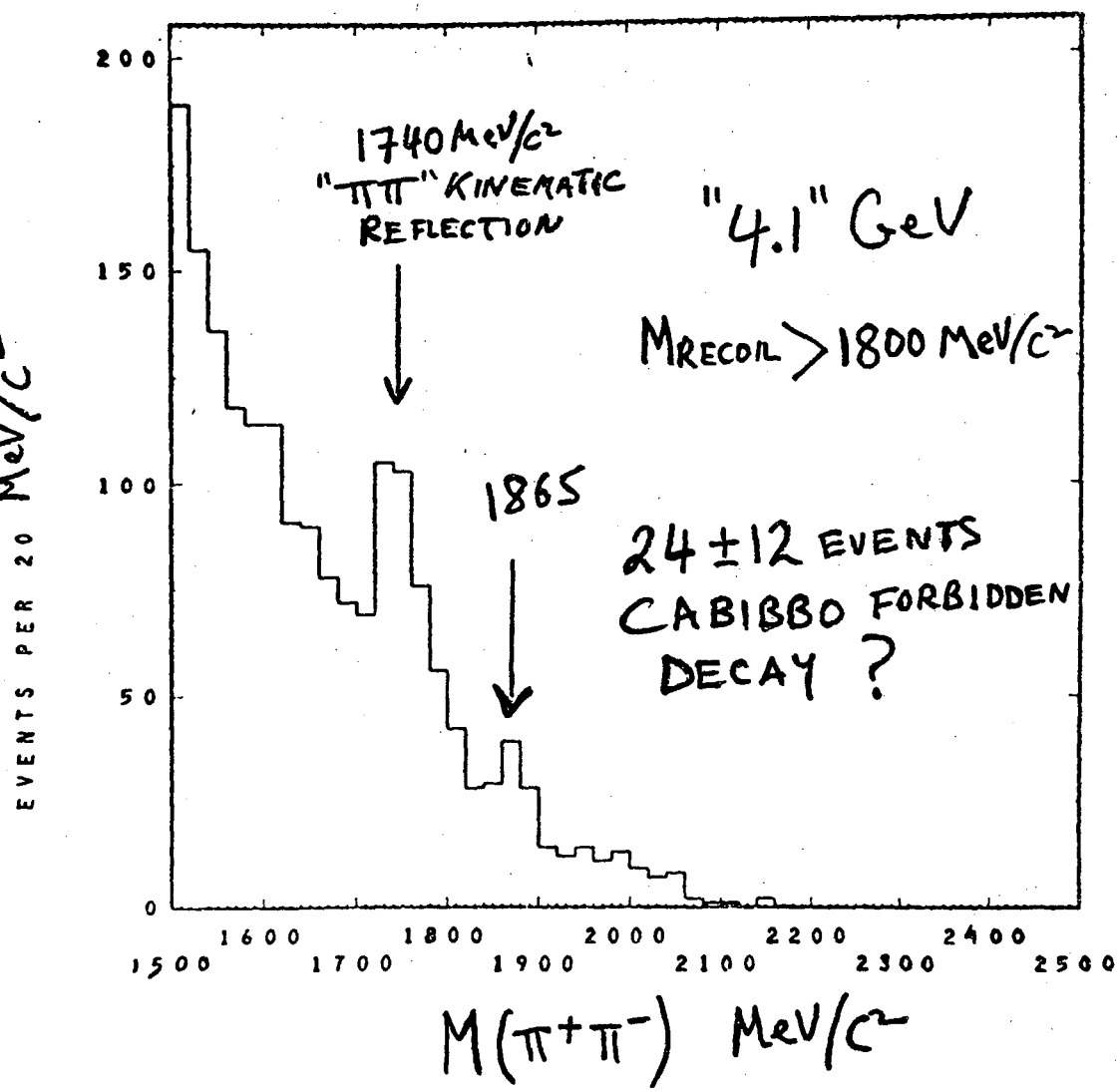
200
150
100
50
0
EVENTS PER 20 MeV/c²
1740 MeV/c²
"ππ" KINEMATIC
REFLECTION
"4.1" GeV
MRECOIL > 1800 MeV/c²
1865
24 ± 12 EVENTS
CABIBBO FORBIDDEN
DECAY ?
1500
1600
1700
1800
1900
2000
2100
2200
2300
2400
2500
M(π⁺π⁻) MeV/c²

Fig. 22

TECHNICAL INFORMATION DIVISION
LAWRENCE BERKELEY LABORATORY
UNIVERSITY OF CALIFORNIA
BERKELEY, CALIFORNIA 94720